IEEE Access
Multidisciplinary | Rapid Review | Open Access Journal

Received December 16, 2019, accepted February 25, 2020, date of publication March 5, 2020, date of current version March 17, 2020.

Digital Object Identifier 10.1109/ACCESS.2020.2978578

Tri-Copter UAV With Individually Tilted Main Wings for Flight Maneuvers

KYUNG-JAE NAM[1], JOOSANG JOUNG[2], AND DONGSOO HAR[1], (Senior Member, IEEE)
[1]Cho Chun Shik Graduate School of Green Transportation, Korea Advanced Institute of Science and Technology (KAIST), Daejeon 34141, South Korea
[2]Department of Aerospace engineering, Korea Advanced Institute of Science and Technology (KAIST), Daejeon 34141, South Korea

Corresponding author: Dongsoo Har (dshar@kaist.ac.kr)

This work was supported by the Ministry of Science and ICT (MSIT), South Korea, through the Information Technology Research Center (ITRC) Support Program supervised by the Institute for Information and communications Technology Planning and Evaluation (IITP) under Grant IITP-2019-2016-0-00314.

ABSTRACT A tri-copter unmanned aerial vehicle (UAV) with individually tilted main wings for various flight maneuvers is presented. In contrast to conventional tilt wing UAVs, thrust vectoring and control of the directions of main wing surfaces are attained by tilting main wings individually. Such individually tilted main wings allow more efficient maneuvers of the UAV. Even though the UAV is a tri-copter, it can compensate the reaction torque created by the tail motor by the individual control of the main wings. Few publications have appeared in the literature, dealing with tri-copter UAV with individually tilted main wings. Dynamic model of the UAV is established via the Newton-Euler formulation and effect of individual wing control is examined. The PID controller and PI controller for control of flight maneuvers are implemented and used for simulations and experiments. Results of simulations and experiments are presented for validation of flight performance of the UAV, including the roll rate 80% larger than that of the conventional UAV with ailerons as control surfaces.

INDEX TERMS Tri-copter, tilt wing UAV, individually tilted main wings, reaction torque, flight performance.

I. INTRODUCTION

Unmanned aerial vehicles (UAVs) have been widely developed and used for various tasks such as disaster assessment [1], airway transportation [2], military aerial vehicles [3], surveillance [4], and logistics [5]. The UAVs are classified into three main categories: fixed wing UAV [6], [7], vertical take-off and landing (VTOL) UAV [8], and hybrid UAV [9], [10]. The fixed wing UAVs have been studied as a classic type of air vehicle. They are able to fly over a long distance at high speed and have mechanical simplicity as compared to other types of UAVs [6], [7]. On the other hand, the fixed wing UAVs require long runway for take-off and landing or dedicated launch system for take-off. The VTOL UAVs are able to perform vertical take-off and landing without the runway and launch system. Due to their handy hovering, they are often used for video recording [11]. However, the VTOL UAVs are structurally complex and have relatively short operation time. To overcome the disadvantages of fixed wing UAVs and VTOL UAVs, hybrid UAVs have been developed. Because of the capability of dual mode flight, the hybrid UAVs are becoming a popular type of UAV.

Hybrid UAV is typically classified into convertiplane [3], [12]–[19] and tail sitter [5], [19]–[26] according to transition mechanism and mechanical configuration. The convertiplane has capabilities of take-off, hovering, cruise flight, and landing without tilting main fuselage during the transition between vertical flight and horizontal flight. The convertiplane is further divided into four sub-categories: tilt rotor UAV, tilt wing UAV, rotor wing UAV, and dual system UAV. The tilt rotor UAV has multiple rotors connected to a rotating shaft. These rotors gradually tilt forward, providing the airplane's forward thrust during the transition [13], [15], [27]. Operation of the tilt wing UAV is similar to that of the tilt rotor UAV, except that the tilt wing UAV tilts their wings together with the rotors [18], [28], [29]. Rotary wings of the rotor wing UAV spin to provide lift force in vertical mode and stop to act like fixed wings in horizontal mode [30]. The dual system UAV has multiple rotors for vertical mode and separate rotor for

The associate editor coordinating the review of this manuscript and approving it for publication was Ming Xu.

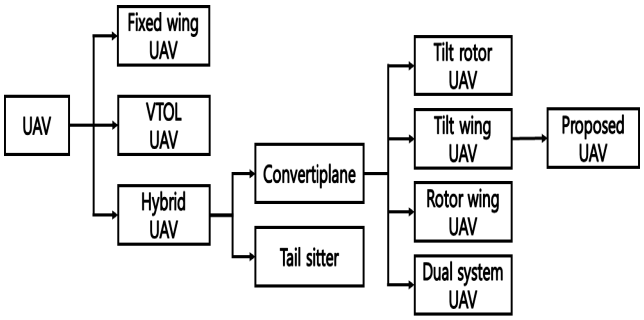

FIGURE 1. Classification of UAVs.

horizontal mode. Classification of the UAVs is summarized in Fig.1.

The tilt wing UAV has high energy efficiency during cruise flight [9]. The energy efficiency and flight endurance are important features especially in the surveillance and emergency situations [31]. Among the tilt wing UAVs, tilt wing UAV of tri-copter type has relative advantages in weight and flight endurance to tilt wing UAV of quad-copter type. However, tilt wing UAV of tri-copter type is generally problematic due to reaction torque [32]–[36]. This UAV typically has unmatched rotor and it generates the torque on the body of the UAV as a consequence. The solutions to this problem are to tilt the unmatched rotor or to use two rotors together to compensate the reaction torque by coaxial reversal [32]–[34]. Other possible solutions include the use of ailerons as control surfaces with additional servo motors to control them.

In this paper, individual control of main wings is proposed to solve the problem of reaction torque with the tilt wing UAV of tri-copter type. Because proposed UAV uses the entire surfaces of the main wings as the control surfaces, more efficient maneuvers can be obtained, as compared to the conventional UAVs that use small control surfaces. As a result, the UAV can compensate reaction torque created by the tail rotor and perform agile roll operation during the horizontal flight. On the other hand, large control surfaces cause instability in control and a problem in transition between vertical mode and horizontal mode [18], [37], [38]. To address these problems, PID controller and PI controller for stable flight operation as well as transition process are developed for the proposed UAV. To the best knowledge of authors, few publications have appeared in the literature, dealing with tilt wing UAV of tri-copter type which is capable of separate control of main wings for various vertical and horizontal flight operations.

This paper is organized as follows. Section II presents design of the UAV. Section III gives prototype and mathematical model of the UAV. Section IV explains the PID controller and PI controller for flight operation and transition between flight modes. Section V presents results of simulations and experiments attempted to show maneuver performance of the UAV. Concluding remarks are in Section VI.

A. CONTRIBUTIONS

The objective of this paper is to develop small size tilt wing UAV of tri-copter type with T-configuration that can compensate reaction torque created by the tail rotor and perform agile flight operations. In a conventional tri-copter, a thrust motor is set to rotate in clockwise direction and the other two spin in counter-clockwise direction and vice versa. The unmatched rotor generates the torque on the body of the UAV as a consequence. Proposed UAV can address the reaction torque by tilting main wings independently. Primary advantage of using entire surfaces of the main wings as the control surfaces lies in more efficient maneuvers that can be obtained during flight. Contributions of this paper are as follows.

1) Design considerations and aerodynamic force analysis of proposed UAV are presented. The aerodynamic force analysis shows large difference of lift force between main wings, which enables agile maneuvers of the UAV.

2) Dynamic model of the UAV is presented. The dynamic model is established based on Newton-Euler formulation. Equations of motion as a part of Newton-Euler formulation are described for the proposed UAV. Agile roll operation of the UAV is accounted for by the equations of motion.

3) The PID controller and PI controller designed for flight operation and mode transition of the UAV are described in details. Control allocation to each actuator (servo motor or BLDC motor) is pictorially explained with proper mathematical validation. Mode transition between horizontal flight and vertical flight is addressed with relevant flow chart.

4) Simulations and experiments demonstrating maneuver performance of the UAV are presented. In the flight simulations, maneuverability comparison of the proposed UAV and typical UAV using ailerons as control surfaces is made with pulse input command. Simulation results show that the maximum roll rate of the proposed UAV is about 2.7rad/s and the UAV with ailerons is about 1.5rad/s, representing 80% improvement over the conventional UAV with ailerons as control surfaces. In the flight experiments, target angles are given by RC transmitter to verify flight stability of the proposed UAV. Experimental results demonstrate that the UAV can perform various maneuvers successfully by compensating reaction torque of the tail motor in windy condition of 4m/s wind speed.

II. DESIGN OF PROPOSED UAV

In this section, mechanical design and aerodynamic analysis of the UAV are presented. Components consisting of front and tail parts of the UAV along with achievable flight operations are explained in subsection II.A. Design considerations include wing surface area and thrust required to achieve cruise speed, both of which are relevant to cruise flight, and lift force pertinent to vertical take-off. Subsection II.B deals with a methodology how to design wings of the UAV with the main concern over wing surface area. Required lift force for vertical take-off is discussed in subsection III.B.

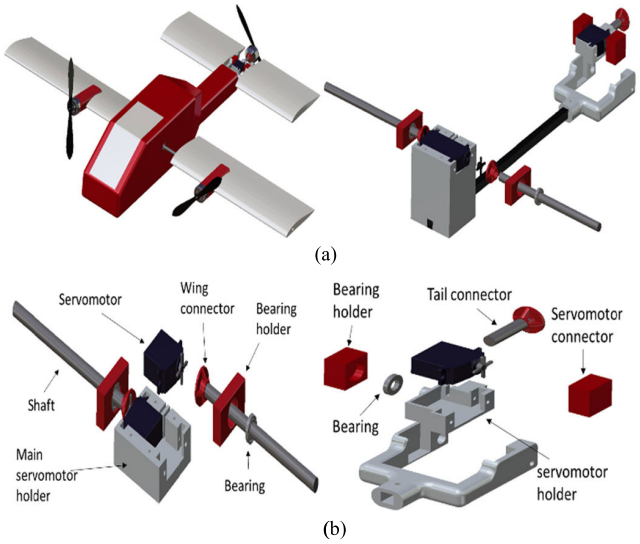

FIGURE 2. Mechanical design of proposed UAV: (a) appearance and structure; (b) detailed structure of front and tail parts.

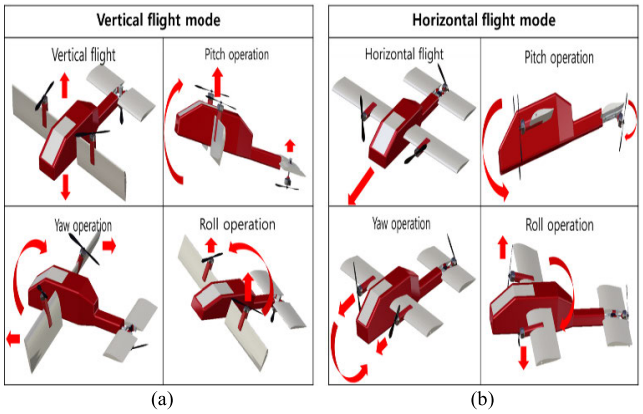

FIGURE 3. Flight operations of proposed UAV: (a) vertical flight mode; (b) horizontal flight mode.

Subsection II.C involves with the aerodynamic force analysis of the UAV.

A. COMPONENTS OF THE UAV AND ACHIEVABLE FLIGHT OPERATIONS

Appearance of the proposed UAV is shown in Fig.2(a) and structure of front part, associated with control of main wings, and tail part, involving rotation of tail BLDC motor, are presented in Fig.2(b). Unlike tilt wings in front part, horizontal stabilizers in tail part are static.

Two BLDC motors are mounted on the main wings and another one is positioned in tail part. The servo motors kept in holders individually rotate main wings and tail BLDC motor. Since a BLDC motor is mounted on each main wing, rotating a main wing also represents adjustment of thrust vectoring. The BLDC motors of front and tail parts rotate propeller blades. The shaft of each wing is connected to each servo motor via wing connector. The bearing and bearing holder in connection with the fuselage support each main wing. The front part makes it possible to tilt the main wings individually. In the tail part, the tail servo motor is connected to the tail BLDC motor by the tail connector and the servo motor holder is held up by bearing and bearing holder. As a result, the tail servo motor can tilt the tail BLDC motor along the shaft of the tail servo motor.

Various flight operations of the UAV are shown in Fig.3. The UAV is able to change the flight mode. Figure 3(a) represents attitude maneuvers in vertical flight mode. They are fulfilled by thrust vectoring of motors on main wings and tail. The thrust vectoring is primarily determined by tilting main wings individually. Conventional tilt wing UAVs that tilt wings in the same direction have a problem in yaw operation, because of the reaction torque generated by the tail motor. The proposed UAV can make yaw movement by tilting the main wings in opposite directions to compensate the reaction torque. It is noted in vertical mode that the tail BLDC motor is erected downward to provide additional lift force. The roll operation is conducted by generating different thrust at each BLDC motor mounted on the main wings. The pitch operation is performed with main wings erected and equal thrust of BLDC motors on the main wings in combination with adequate control of thrust of tail motor. Figure 3(b) shows attitude maneuvers in horizontal flight mode. The yaw operation is attained by different thrusts of the motors on the main wings. The roll operation is achieved by tilting main wings individually, which is in effect thrust vectoring combined with control of the direction of wing surfaces. The pitch operation is adjusted by varying the thrust of the tail BLDC motor.

B. WING DESIGN

The wing loading of the UAV, which is the ratio of weight to wing surface area, determines field performance and maneuverability and the thrust-to-weight ratio decides the thrust to achieve target cruise flight speed [39]. The wing loading with the unit N/m^2 at the stall speed is given by

$$\left(\frac{W}{S}\right)_{stall} = \frac{1}{2}\rho v_{stall}^2 C_{L_{max}} \tag{1}$$

where $W, S, \rho, v_{stall}, C_{L_{max}}$ represent weight of the UAV, wing surface area, air density, stall speed, maximum lift coefficient, respectively. For given weight of the UAV, which is approximately 2×9.8N(ewton), and typical stall speed of small size UAV 12m/s [40] and air density 1.225kg/m^3, the maximum lift coefficient $C_{L_{max}}$ depending on airfoil is necessary to determine the wing surface area S. To get the $C_{L_{max}}$, proper airfoil is selected. When target cruise speed is 20m/s and estimated chord length is about 15cm, the Reynolds number is about 2×10^5 with typical kinematic viscosity for air. The aerodynamic properties of widely used airfoils NACA 0012 [26], NACA 2410 [36], NACA 4412 [6], NACA 23012 [5], and NACA m18 for small size UAVs with the Reynolds number 2×10^5 are considered. Variation of lift coefficient C_L, lift coefficient to drag coefficient

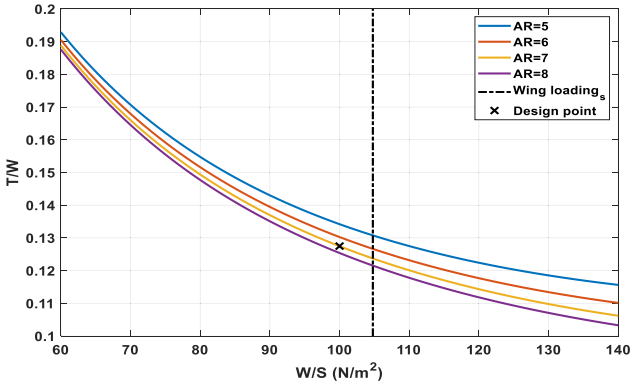

FIGURE 4. The thrust-to-weight ratio(T/W) as a parameterized function of wing loading(w/s). The aspect ratio AR is used as the parameter.

ratio C_L / C_D, and moment coefficient C_M according to the angle of attack are shown in [41] with infinite span wing. In the target range of angle of attack $-10\sim15°$, the NACA 4412 airfoil takes the largest C_L and C_L / C_D. On the other hand, the NACA 4412 airfoil causes large variation of C_M. In case of the NACA m18 airfoil, values of the C_L and C_L / C_D are the second largest and variation of C_M is relatively small. Because large variation of C_M causes flight instability during the transition and horizontal flight, the NACA m18 airfoil is selected, instead of the NACA 4412 airfoil, for the UAV. In [41], the $C_{L_{max}}$ of the NACA m18 airfoil with infinite span wing is approximately 1.32 when the angle of attack is roughly 10°. According to [39], 90% of $C_{L_{max}}$ corresponding to infinite span wing can be used for finite span wing. This discounted value of $C_{L_{max}}$ is used for equation (1).

The thrust-to-weight ratio to achieve target cruise speed in level flight is given in [39] as follows

$$\frac{T}{W} = \frac{1}{2}\rho V_d^2 \frac{C_{D_0}}{(\frac{W}{S})} + \frac{2}{\rho V_d^2} K(\frac{W}{S}) \tag{2}$$

where T, V_d, C_{D_0}, K represent thrust with the unit N, target cruise speed, overall profile drag of UAV, induced drag factor, respectively. The overall profile drag of the UAV is obtained as 0.043 from the aerodynamic analysis presented in subsection II.C. The induced drag factor K is given in [39] by $\frac{1}{\pi(AR)e}$, where AR represents aspect ratio ($\equiv$ total wing span/chord length) and e represents Oswald span efficiency. Empirical equation of Oswald span efficiency with subsonic UAV is given by

$$e = 1.78\left(1 - 0.045\, AR^{0.68}\right) - 0.64 \tag{3}$$

Since the thrust-to-weight ratio in equation (2) is a parameterized function of wing loading in equation (1), variation of the thrust-to-weight ratio can be shown in Fig.4 with the range of parameter AR 5~8. With the discounted $C_{L_{max}}$ =1.32 × 0.9, the wing loading by equation (1) is roughly 105N/m^2. Considering a design margin, wing loading is set to 100N/m^2.

Typically, the AR in the range of 5~8 is considered for small UAVs [40]. Large AR increases the slope of C_L and the value of $C_{L_{max}}$, but decreases the deflection angle causing stall [39]. Because large slope of C_L between two different angles of attack is more favorable to maneuvers of the UAV controlling main wings individually, value of AR is set to 7 with wing loading 100N/m^2. The "x" marked point in Fig.4 at the wing loading 100N/m^2 indicates desired thrust-to-weight ratio.

When the weight of the UAV is 2×9.8N, $0.1962m^2$ of wing surface area is required to satisfy the wing loading 100N/m^2. From this finding, 15cm of wing chord length and 90cm of main wing span as well as 40cm of horizontal stabilizer span are decided, e.g., $0.15\times(0.9+0.4)\approx0.196m^2$. Angle of attack of horizontal stabilizer is set to 3°. With the width of fuselage of the UAV 15cm, the total wing span is 105cm and the AR of the UAV is 7. From the thrust-to-weight ratio 0.1275 matching with wing loading 100N/m^2, as shown in Fig.4, 2.5N of thrust is required for the cruise speed 20m/s. This requirement is considered when the actuators are selected in subsection III.B. Overall design parameters are listed in TABLE 1.

TABLE 1. Parameters of UAV design.

Parameter	Value	Parameter	Value
Assumed weight(mass)	2kg	Wing loading	100N/m^2
Target cruise speed	20m/s	Thrust to weight ratio	0.1275
Stall speed	12m/s	Required wing surface area	0.1962m^2
Air density	1.225kg/m^3	Main wing span	90cm
Chord length	15cm	Horizontal stabilizer span	40cm
Maximum lift coefficient(2D)	1.32	Fuselage width	15cm
Overall profile drag	0.043	Total span	105cm
Aspect ratio	7	Required thrust for cruise flight	2.5N

C. AERODYNAMIC ANALYSIS

The aerodynamic lift force equation is given as follows

$$\text{Lift Force} = \frac{1}{2}\rho v^2 s C_L \tag{4}$$

where v represents airspeed. The force generated by the main wing of the proposed UAV is larger than the force generated by the aileron of conventional UAVs, because large control surface area of main wing is deflected. Large difference of these forces obtained from individually tilted main wings allows agile maneuvers of the UAV. To see the effect of individual control of main wings, flow simulation is conducted by the ANSYS fluent® 15.0 software. For validation of simulation results with the *3-Dimensional* NACA m18 airfoil in Fig.5(a) with 15cm chord length and 45cm half wing span, airfoil data of NACA m18 adopted from [41] are compared as shown in Fig.5(b). Note that both data are

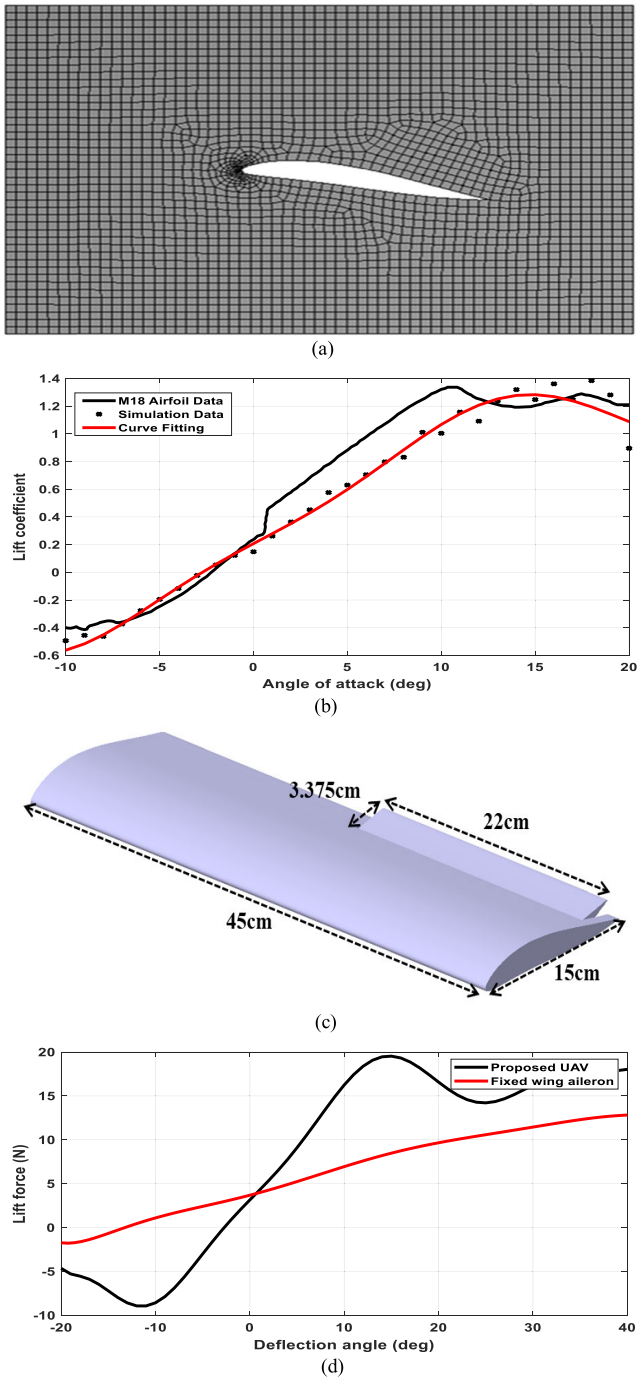

FIGURE 5. Simulation for validation of simulation results and comparison of tilt wing with aileron: (a) NACA m18 airfoil and mesh for validation of simulation results; (b) comparison of simulation results with airfoil data in [41]; (c) wing and aileron used for simulation; (d) lift force generated by tilt wing and aileron.

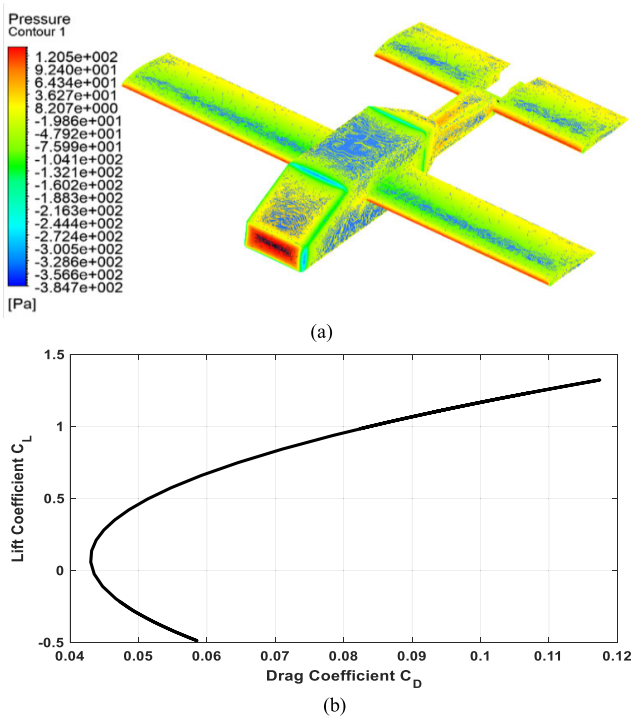

FIGURE 6. Result of aerodynamic analysis and drag polar of the UAV: (a) aerodynamic analysis; (b) drag polar.

obtained with common Reynolds number 2×10^5 and the airfoil shown in Fig.5(a) only shows the cross-section of airfoil with 15cm chord length. As shown in Fig.5(b), simulation results (Simulation Data) are close to airfoil data (M18 Airfoil Data), validating simulation results. However, the maximum lift coefficient $C_{L_{max}}$ and the slope of lift coefficient C_L of simulation results are lower, because of the effect of finite span of wing. Since the simulation results are close to the airfoil data, simulation results obtained from the S/W tool can be considered reliable.

Figure 5(c) shows a wing with a plain flap type of aileron. Relative size of the aileron is determined according to that of the Canadair® CL-84. The relative size of the aileron is within the historical guideline stated in [39]. Deflection angle of tilt wing represents tilt angle of entire wing, while for fixed wing it indicates that of the aileron. Angle of attack of the fixed wing with aileron is set to 0°. As seen in Fig.5(d), large change of lift force occurs according to the deflection angle of tilt wing (Proposed UAV), while aileron (Fixed wing aileron) causes small variation of lift force. Such large difference of lift force between main wings, due to different deflection angles, leads to agile maneuvers of the UAV. As seen in Fig.5(d), wing tilting causes a stall beyond 15° of deflection angle.

In Figure 6(a), aerodynamic analysis of the UAV is presented. It depicts total pressure contour of the UAV with 20m/s inlet airflow speed and 5° of angle of attack. Blue area on the top of fuselage represents relatively low pressure. Pressure difference between top and bottom (not shown here) of the fuselage creates the lift force on the body. Red area in the front of the fuselage represents relatively high pressure. Estimated drag polar of the UAV according to the deflection angle of tilt wing is shown in Fig.6(b) based on the results of aerodynamic analysis. The drag polar shows that overall profile drag C_{D_0}, which is the minimum value of C_D, of the UAV is 0.043.

FIGURE 7. Prototype of proposed UAV.

III. PROTOTYPE AND MATHEMATICAL MODEL

Based on the analytic design process in Section II, prototype of the UAV is to be developed in this section. Mathematical model derived by the Newton-Euler formulation is to prove agile roll maneuver, which represents the most important benefit obtained from individually tilted main wings.

A. PROTOTYPE OF THE UAV

Figure 7 shows the prototype of the proposed UAV. For lightweight structure with mechanical strength, the connectors and holders shown in Fig.2(b) are made up of polylactic acid material. Carbon pipe is used to connect the front part to the tail part, as shown in Fig.2(a). Expanded polypropylene foam is used for the wings. Lightweight isopink foam having high resistance of moisture is used for the fuselage. Horizontal stabilizer is for generation of additional lift force during the transition and horizontal flight. Total span of the prototype is 105cm and chord length is 15cm and total weight of the prototype is 2.03×9.8N.

B. AVIONICS COMPONENTS

The prototype includes various avionics components. Entire avionics of the proposed UAV are shown in Fig.8 and explained as follows.

1) CONTROL BOARD AND SENSORS

The ARM® Cortex M4 with a clock speed 168MHz and computing power of 252MIPS is used as microcontroller. This microcontroller is embedded in a Pixhawk® flight control board. The Pixhawk® control board includes 3-axis L3GD20H 16bit gyroscope, 3-axis ST electronics LSM303D 14bit accelerometer, 3-axis magnetometer, and an MS5611 barometer. A sonar to compensate the uncertainty of the barometer is also aboard. The Neo M8N GPS module in conjunction with the magnetometer provides position information. An analog airspeed sensor is aboard to measure the airspeed during flight.

2) ACTUATORS

The Scorpion® M3011 760kv BLDC motors are used for rotating propellers. Each BLDC motor requires an electric speed controller (ESC). The HobbyKing® 30A ESC is used as motor driver. The APC®10 $\times$ 3.8 composite propellers LP10038SF and LP10038SFP are used to generate thrust for the flight operations. With a combination of propeller and

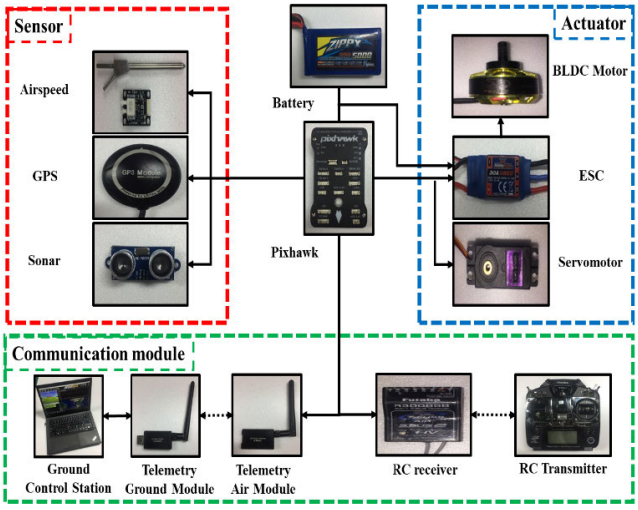

FIGURE 8. Avionics of prototype and relevant communication modules.

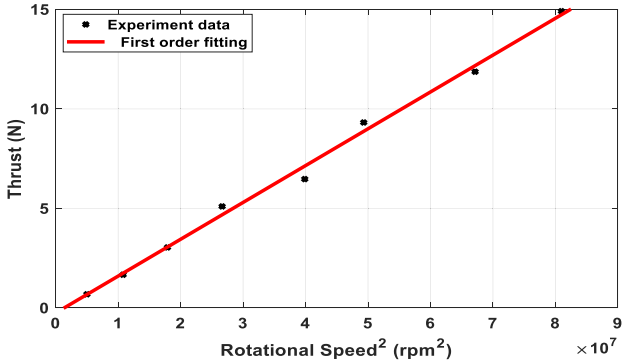

FIGURE 9. Results of thrust experiment.

BLDC motor, experiment to measure thrust is conducted. Results of the thrust experiment are shown in Fig.9.

Since the thrust shown in Fig.9 is obtained with a pair of BLDC motor and propeller, overall thrust of the proposed UAV is 3 times the thrust obtained by the experiment. As a consequence, the required thrust 2.5N for 20m/s desired speed of cruise flight, specified in subsection II.B, and the thrust (≈20N) for the vertical take-off in vertical flight mode are satisfied when the rpm of 3 BLDC motors exceeds around 6500. Results of experiment demonstrate a linear relation between squared rotational speed and thrust as depicted in Fig.9. This linear relationship is expressed as

$$\mathrm{F}_{th} = k\omega^2 \tag{5}$$

where F_{th} and ω represent thrust and rotational speed, respectively. The constant k obtained from the results in Fig. 9 is 1.85×10^{-7}N/rpm^2. The Tower Pro® MG996R servo motor is used to tilt the main wings and tail BLDC motor. It generates 9.40kg·cm torque and provides 60°/0.17s angular speed with holding position between 0 to 18°. All the ESCs and servo motors are controlled by the Pixhawk® control board via its pulse width modulation output.

TABLE 2. Technical specification of prototype.

Parameter	Value
Total weight(mass) without payload	2.03kg
Total span	105cm
Total height	30cm
Total length	80cm
Chord length	15cm
Aspect ratio	7
Maximum thrust	45N
Battery	5000mAh
VTOL endurance	~15min
Maximum flight speed	~21m/s

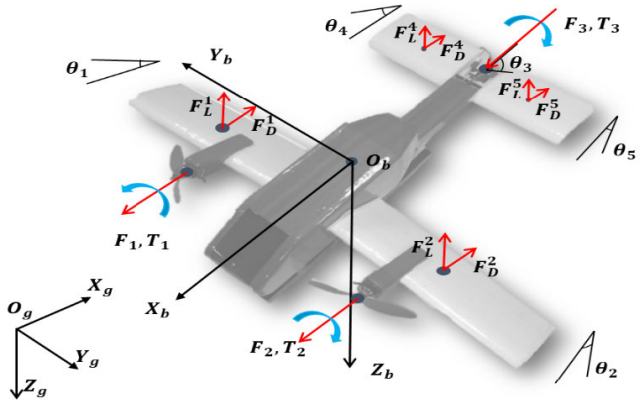

FIGURE 10. Coordinate Frames and external forces relevant to proposed UAV.

3) RC TRANSMITTER/RECEIVER AND TELEMETRY

The Futaba® T10J is used as an RC transmitter to send target angle to the UAV. Futaba® R3008SB is used as the receiver to receive the target angle. Telemetry ground module and telemetry air module are connected by serial communication.

4) BATTERY

The Lightmax®ZIPPY Lithium Polymer (Lipo) 4 cell battery with capacity of 5000mAh and discharge rate 20C is used to supply electric energy to the proposed UAV. Technical specification of the prototype is listed in TABLE 2.

C. MATHEMATICAL MODEL

Dynamic model of the proposed UAV is established via the Newton–Euler formulation. Mathematical expression of individual wing control can explain agile roll maneuver during the horizontal flight.

1) COORDINATE FRAMES

Two reference frames, global frame (O_g, X_g, Y_g, Z_g) and body frame (O_b, X_b, Y_b, Z_b), are considered as in Fig.10. In the global frame, X_g, Y_g, Z_g indicate east, north, downward direction, respectively. The O_g represents the center of the global frame. In the body frame, X_b, Y_b, Z_b indicate front, right, downward direction of the vehicle, respectively. The O_b is the center of mass of the proposed UAV. A rotation matrix $R_{b\to g}$ and a transformation matrix $J_{b\to g}$ [42], [43] that can be used to transfer linear speed and angular speed to the global frame are as follows

$$R_{b\to g} = \begin{bmatrix} c_\psi c_\theta & c_\psi s_\theta s_\phi - s_\psi c_\phi & c_\psi s_\theta c_\phi + s_\psi s_\phi \\ s_\psi c_\theta & s_\psi s_\theta s_\phi + c_\psi c_\phi & s_\psi s_\theta c_\phi - c_\psi s_\phi \\ -s_\theta & c_\theta s_\phi & c_\theta c_\phi \end{bmatrix} \quad (6)$$

$$J_{b\to g} = \begin{bmatrix} 1 & s_\phi s_\theta / c_\theta & c_\phi s_\theta / c_\theta \\ 0 & c_\phi & -s_\phi \\ 0 & s_\phi / c_\theta & c_\phi / c_\theta \end{bmatrix} \quad (7)$$

where ϕ, θ, ψ indicate roll angle, pitch angle, yaw angle of the global frame and $c_{(\cdot)}$, $s_{(\cdot)}$ denote $cos\,(\cdot)$, $sin(\cdot)$, respectively.

2) DYNAMIC EQUATION

Proposed UAV is considered as a rigid body with six degrees of freedom. Dynamic model of the proposed UAV derived via the Newton-Euler formulation can be shown as

$$\begin{bmatrix} mI & 0 \\ 0 & I_b \end{bmatrix} \begin{bmatrix} \dot{V}_b \\ \dot{\Omega}_b \end{bmatrix} + \begin{bmatrix} \Omega_b \times mV_b \\ \Omega_b \times (I_b \Omega_b) \end{bmatrix} = \begin{bmatrix} \mathrm{F}_t \\ \mathrm{M}_t \end{bmatrix} \quad (8)$$

where matrix and vector quantities in the global and body frames are indicated by subscripts g and b, respectively. The mass matrix m is $diag(m, m, m)$ and the inertia matrix of the vehicle I_b is $diag\left(I_{xx}, I_{yy}, I_{zz}\right)$ where I_{xx}, I_{yy}, I_{zz} represent moment of inertia about X_b, Y_b, Z_b-axis, respectively. The identity matrix I and zero matrix 0 are 3×3 matrices. The linear speed in the body frame is denoted as $V_b = [v_x, v_y, v_z]^{\mathrm{T}}$, where the v_x, v_y, v_z represent linear speed along X_b, Y_b, Z_b direction, respectively. The time derivative of linear speed is denoted as $\dot{V}_b$. The angular speed in the body frame is defined as $\Omega_b = [p, q, r]^{\mathrm{T}}$, where p, q, r represent roll rate, pitch rate, yaw rate, respectively. The time derivative of angular speed is denoted as $\dot{\Omega}_b$. The 3×3 matrices F_t and M_t in equation (8) stand for total external forces and moments acting on the center of mass of UAV. These equations defined in the body frame can transform to the global frame by rotational matrix $\mathrm{R}_{b\to g}$ and transformation $J_{b\to g}$ in equations (6), (7) as follows

$$\begin{bmatrix} \dot{P}_g \\ \dot{\Theta}_g \end{bmatrix} = \begin{bmatrix} R_{b\to g} & 0 \\ 0 & J_{b\to g} \end{bmatrix} \begin{bmatrix} V_b \\ \Omega_b \end{bmatrix} \quad (9)$$

where position vector defined in the global frame is denoted as $P_g = [x, y, z]^{\mathrm{T}}$, where the x, y, z represent global position along X_g, Y_g, Z_g directions, respectively. The orientation vector defined in the global frame is denoted as $\Theta_g = [\phi, \theta, \psi]^{\mathrm{T}}$.

3) FORCE EQUATION

Figure 10 shows the external forces and moments generated on the proposed UAV horizontal mode. The total force F_t in equation (8) includes the thrust of the BLDC motors F_{th}, aerodynamic forces on the wings F_w, gravity force on the UAV, and disturbances F_d that come from the environment such as gust. These forces are defined in the body frame as follows

$$\mathrm{F}_t = \mathrm{F}_{th} + \mathrm{F}_w + [-s_\theta, c_\theta s_\phi, c_\theta c_\phi]^{\mathrm{T}} mg + \mathrm{F}_d \quad (10)$$

where

$$\mathrm{F}_{th} = \begin{bmatrix} c_{\theta_1} & c_{\theta_2} & c_{\theta_3} \\ 0 & 0 & 0 \\ -s_{\theta_1} & -s_{\theta_2} & -s_{\theta_3} \end{bmatrix} \begin{bmatrix} k\omega_1^2 \\ k\omega_2^2 \\ k\omega_3^2 \end{bmatrix} \tag{11}$$

where thrust along Y_b direction is 0 and θ_i, where $i = 1,2,3$, denotes tilt angles of main wings and tail BLDC motor with respect to X_b axis of the body frame. The motor thrust $k\omega_i^2$ is obtained by equation (5). The F_w is given by

$$\mathrm{F}_w = \begin{bmatrix} (F_D^1 + F_D^2 + F_D^4 + F_D^5) \\ 0 \\ (F_L^1 + F_L^2 + F_L^4 + F_L^5) \end{bmatrix} \tag{12}$$

where aerodynamic force along Y_b direction is considered as 0. Superscripts 1, 2 represent main wings and 4, 5 indicate horizontal stabilizers. The lift force $F_L^i(\theta_i)$ and drag force $F_D^i(\theta_i)$ of the main wings are expressed in terms of θ_1 and θ_2 and those of the horizontal stabilizers are expressed in terms of θ_4 and θ_5 as following

$$\begin{bmatrix} F_D^i \\ 0 \\ F_L^i \end{bmatrix} = \begin{bmatrix} -\frac{1}{2}\rho v^2 s C_D(\theta_i) \\ 0 \\ -\frac{1}{2}\rho v^2 s C_L(\theta_i) \end{bmatrix} \quad (\text{for } i = 1, 2, 4, 5) \tag{13}$$

where the drag coefficient C_D and lift coefficient C_L are functions of θ_i. The individual wing control produces different angles of attack of the main wings. Different angles of attack of main wings can create large difference of lift force. Note that the angles of attack of horizontal stabilizers are fixed at $\theta_4 = \theta_5 = 3°$.

4) MOMENT EQUATION

The total moment M_t in equation (8) consists of the moments created by the rotors M_{th}, aerodynamic forces generated by the wings M_w, gyroscopic effect in the propellers, and moments due to the external disturbances M_d. The external disturbances include torques created by the aerodynamic forces caused by asymmetric fuselage. The M_t can be described as

$$\mathrm{M}_t = (\mathrm{M}_{th} + \mathrm{M}_w + \sum_{i=1}^{3} J_{prop}[\eta_i \Omega_b \times [c_{\theta_i}, 0, -s_{\theta_i}]^{\mathrm{T}}] + \mathrm{M}_d) \tag{14}$$

where J_{prop} is rotational inertia of rotors about rotor axes and parameter $\eta_i (i = 1, 2, 3)$ indicating rotational direction takes values $-1, 1, 1$ for $i = 1, 2, 3$, respectively. The M_{th} is given as

$$\mathrm{M}_{th} = \begin{bmatrix} -d_{my}s_{\theta_1} + \lambda c_{\theta_1} & d_{my}s_{\theta_2} - \lambda c_{\theta_2} & -\lambda c_{\theta_3} \\ d_{mx}s_{\theta_1} - d_{mz}c_{\theta_1} & d_{mx}s_{\theta_2} - d_{mz}c_{\theta_2} & -d_{tx}s_{\theta_3} + d_{tz}c_{\theta_3} \\ -d_{my}c_{\theta_1} - \lambda s_{\theta_1} & d_{my}c_{\theta_2} + \lambda s_{\theta_2} & \lambda s_{\theta_3} \end{bmatrix} \times \begin{bmatrix} k\omega_1^2 \\ k\omega_2^2 \\ k\omega_3^2 \end{bmatrix} \tag{15}$$

where d indicates projected distance between each BLDC motor and center of mass of the UAV. Subscripts m, t, x, y, and z indicate a BLDC motor mounted on a main wing, BLDC motor in tail part, x direction, y direction, and z direction in the body frame, respectively. For example, d_{my} means the y-projected distance between the BLDC motor mounted on the main wing and center of mass of the UAV. Reaction torque of the i-th rotor is defined as $T_i = \lambda k\omega_i^2$, where the λ is the torque/force ratio of the rotor. Range of λ for typical propeller used for small UAV is 0.01-0.05 [36]. The M_w is given by

$$\mathrm{M}_w = \begin{bmatrix} -\ell_{wy}(F_L^1 - F_L^2) - \ell_{ty}(F_L^4 - F_L^5) \\ \ell_{wx}(F_L^1 + F_L^2) - \ell_{tx}(F_L^4 + F_L^5) - \ell_{tz}(F_D^4 + F_D^5) \\ \ell_{wy}(F_D^1 - F_D^2) + \ell_{ty}(F_D^4 - F_D^5) \end{bmatrix} \tag{16}$$

where the ℓ indicates distance between each wing and center of mass of the UAV. Subscript w, t indicate center of wing, center of stabilizer, respectively. For example, ℓ_{ty} represents projected distance between each center of stabilizer and center of mass of the UAV along Y_b-axis. Due to symmetricity of the UAV along X_b-axis, ℓ_{ty} for left wing and ℓ_{ty} for right wing are identical. The moment M_t in equation (14) can be expressed as $[M_x, M_y, M_z]^{\mathrm{T}}$, where the M_x, M_y, M_z represent the moments creating roll, pitch, yaw operations, respectively, neglecting gyroscopic effect and external disturbances, and shown as follows

$$\begin{aligned} M_x &= -\mathrm{d}_{\mathrm{my}}(F_1 s_{\theta_1} - F_2 s_{\theta_2}) + T_1 c_{\theta_1} - T_2 c_{\theta_2} - T_3 c_{\theta_3} \\ &\quad - \ell_{wy}\left(F_L^1 - F_L^2\right) - \ell_{ty}(F_L^4 - F_L^5) \end{aligned} \tag{17}$$

$$\begin{aligned} M_y &= \mathrm{d}_{mx}(F_1 s_{\theta_1} + F_2 s_{\theta_2}) - \mathrm{d}_{mz}(F_1 c_{\theta_1} + F_2 c_{\theta_2}) \\ &\quad - \mathrm{d}_{tx} F_3 s_{\theta_3} + \mathrm{d}_{tz} F_3 c_{\theta_3} + \ell_{wx}\left(F_L^1 + F_L^2\right) - \ell_{tx}(F_L^4 + F_L^5) \\ &\quad - \ell_{tz}(F_D^4 + F_D^5) \end{aligned} \tag{18}$$

$$\begin{aligned} M_z &= -\mathrm{d}_{my}(F_1 c_{\theta_1} - F_2 c_{\theta_2}) - T_1 s_{\theta_1} + T_2 s_{\theta_2} + T_3 s_{\theta_3} \\ &\quad + \ell_{wy}\left(F_D^1 - F_D^2\right) + \ell_{ty}\left(F_D^4 - F_D^5\right) \end{aligned} \tag{19}$$

In the horizontal flight, moment M_x creating rotation about X_b -axis is concerned with roll operation. Euler equation in equation (8) for roll operation in the body frame can be expressed as follows

$$\dot{p} = \frac{1}{I_{xx}}\{(I_{yy} - I_{zz})\, qr + M_x\} \tag{20}$$

The transformation equation from body to global frame in equation (9) for roll operation is defined as follows

$$\dot{\phi} = p + s_\phi s_\theta / c_\theta q + c_\phi s_\theta / c_\theta r \tag{21}$$

When pitch and yaw operations are stable, the pitch rate q and yaw rate r defined in the body frame are close to 0. Therefore, equations (20) and (21) can be expressed as $\dot{p} \approx M_x / I_{xx}$ and $\dot{\phi} \approx p = \int \dot{p} dt$. Because the effects of thrust and torque in equation (17), e.g., $-d_{my}(F_1 s_{\theta_1} - F_2 s_{\theta_2}) + T_1 c_{\theta_1} - T_2 c_{\theta_2} - T_3 c_{\theta_3}$, are relatively small during the cruise flight, wing

TABLE 3. Projected distances and moment of inertia.

Parameter	Value
X_b-directional projected distance between center of mass and each BLDC motor of main wing (d_{mx})	15cm
Y_b-directional projected distance between center of mass and each BLDC motor of main wing (d_{my})	26cm
Z_b-directional projected distance between center of mass and each BLDC motor of main wing (d_{mz})	1cm
X_b-directional projected distance between center of mass and tail BLDC motor (d_{tx})	30cm
Z_b-directional projected distance between center of mass and tail BLDC motor (d_{tz})	11cm
X_b-directional projected distance between center of mass and center of each main wing (l_{wx})	14cm
Y_b-directional projected distance between center of mass and center of each main wing (l_{wy})	30cm
X_b-directional projected distance between center of mass and center of each horizontal stabilizer (l_{tx})	31cm
Y_b-directional projected distance between center of mass and center of each horizontal stabilizer (l_{ty})	15cm
Z_b-directional projected distance between center of mass and center of each horizontal stabilizer (l_{tz})	4cm
Moment of inertia about X_b-axis (I_{xx})	0.0569kg · m^2
Moment of inertia about Y_b-axis (I_{yy})	0.1058kg · m^2
Moment of inertia about Z_b-axis (I_{zz})	0.1304kg · m^2

forces become critical. The equation (21) together with equations (17), (20) can be rewritten as follows

$$\dot{\phi} \approx \int \{\left[-\ell_{wy}\left(F_L^1 - F_L^2\right) - \ell_{ty}\left(F_L^4 - F_L^5\right)\right]/I_{xx}\}dt \qquad (22)$$

Individual control of main wings can make different angles of attack of main wings. When main wings are tilted in opposite directions, the $|F_L^1 - F_L^2|$ in equation (22) becomes large, causing agile roll operation. It is noted that $|F_L^1 - F_L^2| \gg |F_L^4 - F_L^5|$ due to significantly larger main wings.

The projected distances between center of mass of the UAV and each BLDC motor, projected distances between center of mass of the UAV and each wing, and moment of inertia about each axis are listed in TABLE 3.

IV. CONTROL MODEL AND TRANSITION PROCESS

To achieve flight stability in vertical and horizontal flight modes, the Ardupilot code on the Pixhawk® board is modified for the implementation of the controllers. These controllers are implemented with several parameters related to the propulsion system, aerodynamic forces, gravity force, and disturbances. Allocations of the outputs of PID controller/PI controller to six actuators(motors) are configured to be fit to the attitude maneuvers of the UAV. Mathematical validation for the output allocation, similar to those in [44]–[46], is presented in this section, considering that the main difference of control model for the proposed UAV is to allocate distinct outputs to two motors for main wings. The transition process from the vertical mode to the horizontal mode is customized to serve the flight operations of the proposed UAV. It is possible to use VTOL configuration of the Ardupilot in the vertical flight. However, without the modification, forward transition and horizontal flight of the proposed UAV performing individual control of main wings cannot be performed properly. The code of the Ardupilot for roll operation in the horizontal flight should be modified, due to individual control of main wings. Also, because proposed UAV does not have an elevator, the code for the pitch operation during the horizontal flight and transition needs to be modified. Tilting entire wing surfaces or tail motor increases the agility of the flight, but it reduces stability during the horizontal flight and forward transition. This requires additional modification of the code. The transition process from the vertical mode to the horizontal mode is customized. In this section, control model with output allocation and transition process are presented.

A. CONTROL MODEL FOR VERTICAL FLIGHT MODE

The external moment equation suitable for hovering state in vertical mode is as follows. The equation (17) corresponding to roll operation can be approximated by $\mathrm{d}_{my}\left(F_1 s_{\theta_1} - F_2 s_{\theta_2}\right)\left[= -\mathrm{d}_{my}\left(k\omega_1^2 - k\omega_2^2\right)\right]$, because small λ of $T_i (i = 1, 2, 3)$ and wing lift force $F_L^i (i = 1, 2, 4, 5)$ are negligible. The $s_{\theta_1}(= sin(\theta_1))$ and $s_{\theta_2}(= sin(\theta_2))$ are 1, since $\theta_1 = \theta_2 = 90°$ in roll operation. Therefore, $T_1 c_{\theta_1} - T_2 c_{\theta_2} - T_3 c_{\theta_3} - \ell_{wy}\left(F_L^1 - F_L^2\right) - \ell_{ty}\left(F_L^4 - F_L^5\right)$ is significantly smaller than $\mathrm{d}_{my}\left(F_1 s_{\theta_1} - F_2 s_{\theta_2}\right)$ and thus can be neglected. The equation (18) accounting for pitch operation can also be approximated by $\mathrm{d}_{mx}\left(F_1 s_{\theta_1} + F_2 s_{\theta_2}\right) - \mathrm{d}_{tx} F_3 s_{\theta_3}\left[= \mathrm{d}_{mx}\left(k\omega_1^2 + k\omega_2^2\right) - \mathrm{d}_{tx} k\omega_3^2\right]$, because $c_{\theta_1}(=cos(\theta_1))$ and $c_{\theta_2}(=cos(\theta_2))$ and $c_{\theta_3}(=cos(\theta_3))$ are 0 with $\theta_1 = \theta_2 = \theta_3 = 90°$ in pitch operation and $\ell_{wx}\left(F_L^1 + F_L^2\right) - \ell_{tx}(F_L^4 + F_L^5) - \ell_{tz}\left(F_D^4 + F_D^5\right)$ is significantly smaller than $\mathrm{d}_{mx}\left(F_1 s_{\theta_1} + F_2 s_{\theta_2}\right) - \mathrm{d}_{tx} F_3 s_{\theta_3}\left[= \mathrm{d}_{mx}\left(k\omega_1^2 + k\omega_2^2\right) - \mathrm{d}_{tx} k\omega_3^2\right]$. The equation (19) corresponding to yaw operation can be approximated by $\mathrm{d}_{my}\left(F_1 c_{\theta_1} - F_2 c_{\theta_2}\right) + T_3 s_{\theta_3}[= -\mathrm{d}_{my}\left(k\omega_1^2 c_{\theta_1} - k\omega_2^2 c_{\theta_2}\right) + \lambda k\omega_3^2]$. The $-T_1 s_{\theta_1} + T_2 s_{\theta_2}$ becomes 0 due to the relationship $\theta_1 = 90° - \Delta$, $\theta_2 = 90° + \Delta$ and $\ell_{wy}\left(F_D^1 - F_D^2\right) + \ell_{ty}\left(F_D^4 - F_D^5\right)$ is significantly smaller than $-\mathrm{d}_{my}\left(F_1 c_{\theta_1} - F_2 c_{\theta_2}\right) + T_3 s_{\theta_3}$. From foregoing discussion, the M_x, M_y, M_z in equations (17), (18), (19) can be rewritten as follows

$$M_x = -\mathrm{d}_{my}(k\omega_1^2 - k\omega_2^2) \qquad (23)$$

$$M_y = \mathrm{d}_{mx}\left(k\omega_1^2 + k\omega_2^2\right) - \mathrm{d}_{tx} k\omega_3^2 \qquad (24)$$

$$M_z = -\mathrm{d}_{my}\left(k\omega_1^2 c_{\theta_1} - k\omega_2^2 c_{\theta_2}\right) + \lambda k\omega_3^2 \qquad (25)$$

As seen in the equation of M_x in equation (23), rotational speed of right BLDC motor ω_1 and rotational speed of left BLDC motor ω_2 are required for roll operation. The M_y accounting for variation of pitch operation is pertinent to the rotation about Y_b-axis. For M_y in equation (24), $\omega_1, \omega_2, \omega_3$ are required. The reaction torque in vertical flight mode of the

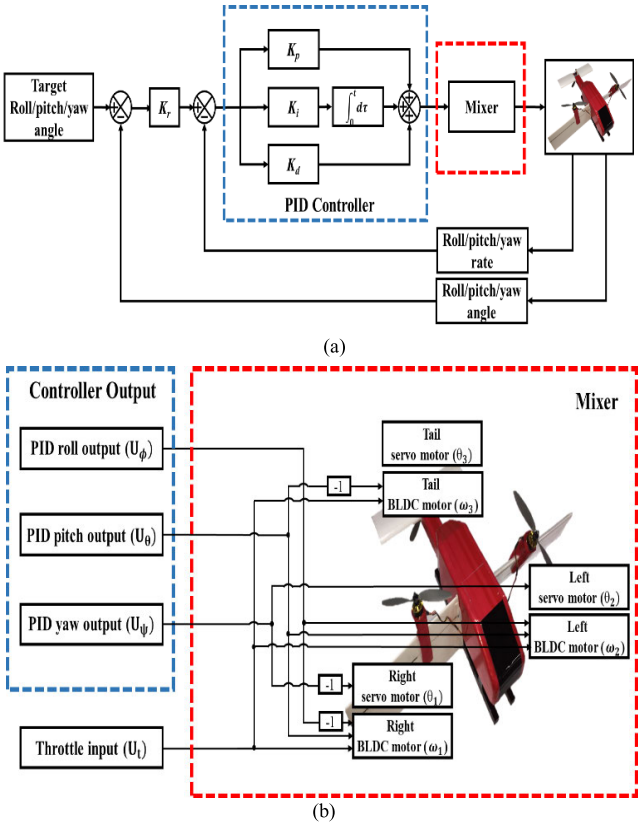

FIGURE 11. Vertical flight controller and mixer: (a) PID controller for attitude operations; (b) vertical flight mode mixer.

UAV is compensated during yaw operation. For the compensation of reaction torque during yaw operation, the 3rd term in equation (25) accounting for the reaction torque $T_3 = \lambda k\omega_3^2$ should satisfy $T_3 = \mathrm{d}_{wy}\left(k\omega_1^2 c_{\theta_1} - k\omega_2^2 c_{\theta_2}\right)$. It is noted that in yaw operation the angles of servo motors θ_1, θ_2 can be acute or obtuse.

The vertical flight mode of the proposed UAV is executed by the control of the PID controller. Figure 11 shows the functional block diagrams for the attitude control and mixer for flight operations in the vertical mode. Figure 11(a) shows the PID controller for roll, pitch, and yaw operations in vertical mode. The PID controller controls the power of every motor, except the tail servo motor, to meet the target angle in vertical mode. In vertical mode, the tail BLDC motor is always erected downward. For each operation, the PID controller for vertical flight can be given as follows

$$U_\phi = K_{p,\phi}\,(p_t - p) + K_{i,\phi}\int (p_t - p) + K_{d,\phi}(p_t - p) \tag{26}$$

$$U_\theta = K_{p,\theta}\,(q_t - q) + K_{i,\theta}\int (q_t - q) + K_{d,\theta}(q_t - q) \tag{27}$$

$$U_\psi = K_{p,\psi}\,(r_t - r) + K_{i,\psi}\int (r_t - r) + K_{d,\psi}(r_t - r) \tag{28}$$

where U_ϕ, U_θ, U_ψ represent the outputs of each PID controllers for roll, pitch, yaw operation, respectively. The K_p, K_i, K_d represent the gains of the PID controller. Subscript ϕ, θ, ψ respectively indicate roll, pitch, yaw operation. The p, q, r represent the roll rate, pitch rate, and yaw rate in the body frame, respectively. Subscript t in equations (26), (27), (28) represent target values. Target angle is given by RC transmitter and consequent target rate is evaluated from target angle. For example, target yaw rate $r_t = K_r\,(\psi_t - \psi)$ where the gain K_r is a proportional constant in conversion of yaw angle error to target yaw rate. Each output of the PID controller and throttle input U_t, given by the RC transmitter, go to the mixer shown in Fig.11(b). The mixer represents all the connections between the outputs of the PID controller and actuators and between throttle input and BLDC motors. From foregoing procedures, control allocation to 3 servo motors and 3 BLDC motors can be given as follows

TABLE 4. Gains of PID controllers for vertical flight mode.

	K_p	K_i	K_d
Roll	0.38	0.08	0.017
Pitch	0.32	0.16	0.0036
Yaw	0.22	0.01	0.04

$$\omega_1 = -U_\phi + U_\theta + U_t \tag{29}$$

$$\omega_2 = U_\phi + U_\theta + U_t \tag{30}$$

$$\omega_3 = -U_\theta + U_t \tag{31}$$

$$\theta_1 = 90^\circ - U_\psi \tag{32}$$

$$\theta_2 = 90^\circ + U_\psi \tag{33}$$

$$\theta_3 = 90^\circ \tag{34}$$

The rotational speeds of right and left BLDC motors ω_1, ω_2 determine the moment creating roll operation in vertical flight mode as described in equation (23). Considering the mechanism of roll operation, output of the PID controller in charge of roll operation U_ϕ goes to the right BLDC motor with negative sign and goes to the left BLDC motor. Other terms U_θ, U_t are commonly taken for ω_1, ω_2. As a consequence, differential rotational speed of right BLDC motor with respect to left BLDC motor creates roll operation described in equation (23). In case of pitch operation in equation (24), the output of the PID controller for pitch operation U_θ should be commonly used to determine $\omega_1, \omega_2, \omega_3$. Direction of pitch operation, either nose up or nose down, is determined by the rotational speed of tail BLDC motor ω_3 relative to ω_1, ω_2, as shown in equation (24). For yaw operation, tilt angle of right servo motor θ_1 is $90^\circ - U_\psi$ and tilt angle of left servo motor θ_2 is $90^\circ + U_\psi$, as expected. Tilt angle of tail servo motor during vertical flight is fixed at $\theta_3 = 90^\circ$. The adjustment of angles $\theta_1, \theta_2, \theta_3$ with the bias 90° is not shown in Fig.11(b). The gains K_p, K_i, K_d of PID controllers for vertical flight mode are listed for each operation in TABLE 4.

B. CONTROL MODEL FOR HORIZONTAL FLIGHT MODE

The external moment equation suitable for cruise flight in horizontal mode is as follows. During cruise flight, main wings affect the flight operation significantly more than the stabilizer, because of much larger wing size. The equation (17) corresponding to roll operation can be approximated by $-\ell_{wy}\left(F_L^1 - F_L^2\right) - \ell_{ty}\left(F_L^4 - F_L^5\right)$, because F_i is relatively small during the cruise flight and small λ of T_i $(i = 1, 2, 3)$ makes T_i negligible. It is noted that the sum of thrusts $F_1 + F_2 + F_3$ for cruise flight is about 2.4N, whereas the sum of thrusts for hovering is about 20N as mentioned in subsection III.B. Therefore, $-d_{my}(F_1 s_{\theta_1} - F_2 s_{\theta_2}) + T_1 c_{\theta_1} - T_2 c_{\theta_2} - T_3 c_{\theta_3}$ is significantly smaller than $-\ell_{wy}\left(F_L^1 - F_L^2\right) - \ell_{ty}(F_L^4 - F_L^5)$ and thus can be neglected. The equation (18) accounting for pitch operation can also be approximated by $-\mathrm{d}_{tx} F_3 s_{\theta_3} + \mathrm{d}_{tz} F_3 c_{\theta_3} [= -\mathrm{d}_{tx} k\omega_3^2 s_{\theta_3} + \mathrm{d}_{tz} k\omega_3^2 c_{\theta_3}]$ for thrust vectoring, because small F_i $(i = 1, 2)$ in $\mathrm{d}_{mx}\left(F_1 s_{\theta_1} + F_2 s_{\theta_2}\right) - \mathrm{d}_{mz}\left(F_1 c_{\theta_1} + F_2 c_{\theta_2}\right)$ and $\ell_{wx}\left(F_L^1 + F_L^2\right) - \ell_{tx}(F_L^4 + F_L^5) - \ell_{tz}(F_D^4 + F_D^5) \approx 0$ for the longitudinal static stability [39] are negligible. Therefore, $\mathrm{d}_{mx}\left(F_1 s_{\theta_1} + F_2 s_{\theta_2}\right) - \mathrm{d}_{mz}\left(F_1 c_{\theta_1} + F_2 c_{\theta_2}\right) + \ell_{wx}\left(F_L^1 + F_L^2\right) - \ell_{tx}(F_L^4 + F_L^5) - \ell_{tz}(F_D^4 + F_D^5)$ is significantly smaller than $-\mathrm{d}_{tx} k\omega_3^2 s_{\theta_3} + \mathrm{d}_{tz} k\omega_3^2 c_{\theta_3}$. The equation (19) corresponding to yaw operation can be approximated by $-\mathrm{d}_{my}\left(F_1 c_{\theta_1} - F_2 c_{\theta_2}\right) [= -\mathrm{d}_{my}\left(k\omega_1^2 c_{\theta_1} - k\omega_2^2 c_{\theta_2}\right)]$, because small λ of T_i $(i = 1, 2, 3)$ is negligible and the angles of wings during the cruise flight are static and equal to each other, i.e., $F_D^1 = F_D^2$. Therefore, $-T_1 s_{\theta_1} + T_2 s_{\theta_2} + T_3 s_{\theta_3}$ and $\ell_{wy}\left(F_D^1 - F_D^2\right) + \ell_{ty}\left(F_D^4 - F_D^5\right)$ are significantly smaller than $-\mathrm{d}_{my}\left(F_1 c_{\theta_1} - F_2 c_{\theta_2}\right) \left[= -\mathrm{d}_{my}\left(k\omega_1^2 c_{\theta_1} - k\omega_2^2 c_{\theta_2}\right)\right]$. From foregoing discussion, the M_x, M_y, M_z in equations (17), (18), (19) can be rewritten as follows

$$M_x = -\ell_{wy}\left(F_L^1 - F_L^2\right) - \ell_{ty}\left(F_L^4 - F_L^5\right) \tag{35}$$

$$M_y = -\mathrm{d}_{tx} k\omega_3^2 s_{\theta_3} + \mathrm{d}_{tz} k\omega_3^2 c_{\theta_3} \tag{36}$$

$$M_z = -\mathrm{d}_{my}\left(k\omega_1^2 c_{\theta_1} - k\omega_2^2 c_{\theta_2}\right) \tag{37}$$

As seen in the equation of M_x in equation (35), wing forces of F_L^1, F_L^2, are functions of tilt angles of right servo motor θ_1 and tilt angle of left servo motor θ_2, respectively. It is noted that $|F_L^1 - F_L^2| \gg |F_L^4 - F_L^5|$ during the roll operation in horizontal flight, due to significantly small stabilizers, as compared to main wings. The M_y accounting for pitch operation is pertinent to the rotation about Y_b-axis. For M_y in equation (36), θ_3, ω_3 are required for thrust vectoring. For the M_z in equation (37), rotational speed of right BLDC motor ω_1 and rotational speed of left BLDC motor ω_2 are required for yaw operation.

The horizontal flight mode of the proposed UAV is executed by the control of the PID controller and PI controller. Figure 12 shows the functional block diagrams for the attitude control and mixer for flight operations in the horizontal mode. Attitude control by the PID controller is shown in Fig.12(a-b) and that by the PI controller is depicted in Fig.12(c). There are target angles set for the roll and pitch operations whereas target angle is not set for yaw operation. Figure 12(a) shows the part of PID controller relevant to roll operation. The roll output U_ϕ is mathematically

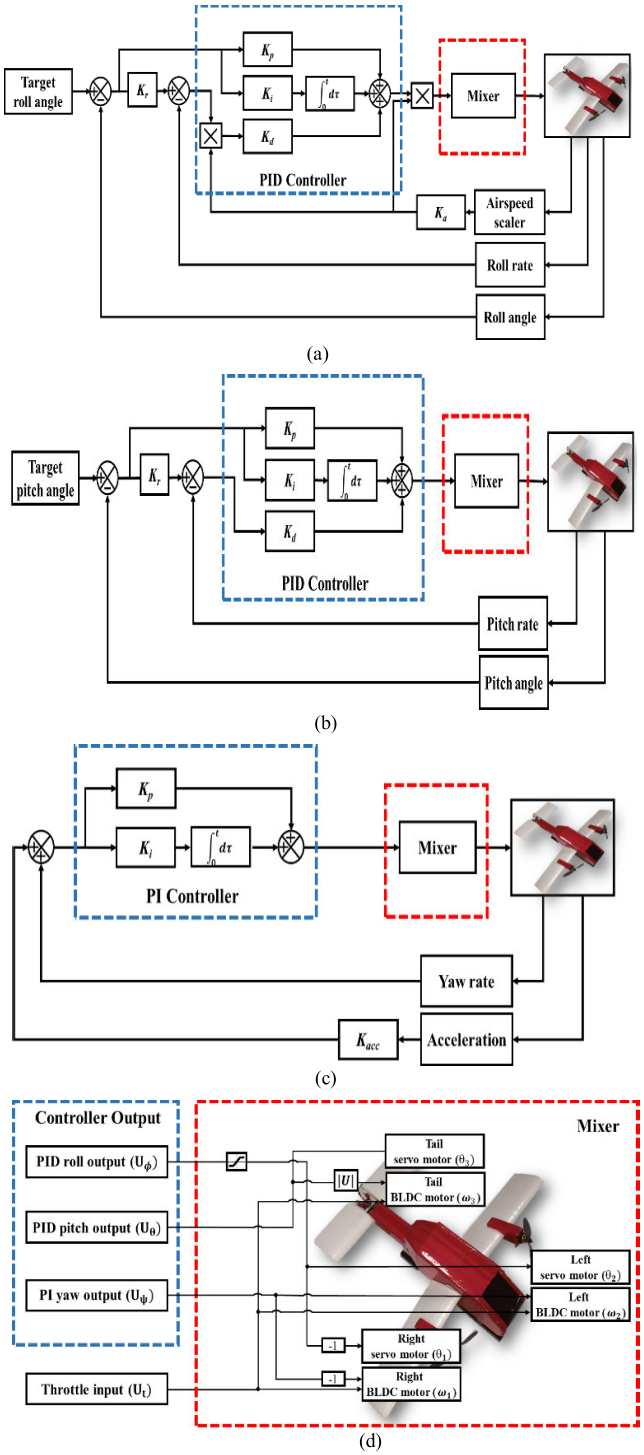

FIGURE 12. Horizontal flight controller and mixer: (a) PID controller for roll operation; (b) PID controller for pitch operation; (c) PI controller for yaw operation; (d) horizontal flight mode mixer.

presented as

$$U_\phi = \frac{K_a}{v}[K_{p,\phi}\,(\phi_t - \phi) + K_{i,\phi}\int(\phi_t - \phi) + K_{d,\phi}\{\frac{K_a}{v}\,(p_t - p)\}] \quad (38)$$

where the ϕ_t and ϕ represent the target pitch angle given by the RC transmitter and pitch angle of UAV. The p_t, p, v and K_a represent the target roll rate, roll rate of the UAV, airspeed, and gain for airspeed, respectively. Figure 12(b) shows the part of PID controller relevant to pitch operation. The pitch output U_θ is presented as

$$U_\theta = K_{p,\theta}\,(\theta_t - \theta) + K_{i,\theta}\int(\theta_t - \theta) + K_{d,\theta}(q_t - q) \quad (39)$$

where θ_t and θ represent the target pitch angle given by the RC transmitter and pitch angle of UAV. The q_t and q represent the target pitch rate and pitch rate of the UAV. Tilting main wings individually for roll operation generates uneven drag force and thus creates the sideslip [47]. The UAV reduces the sideslip during roll operation by accompanied yaw operation executed by the PI controller. In Fig.12(c), the yaw rate and Y_b-direction acceleration are appropriately adjusted by the PI controller. The yaw output U_ψ is obtained as

$$U_\psi = K_{p,\psi}(K_{acc}a_y + r) + K_{i,\psi}\int\left(K_{acc}a_y + r\right) \quad (40)$$

where K_{acc} represents gains for Y_b-directional acceleration, and a_y, r are Y_b-directional acceleration, yaw rate in the body frame, respectively. Outputs of the PID controller/PI controller and throttle input go to the mixer shown in Fig.12(d). From foregoing procedures, control allocation to 3 servo motors and 3 BLDC motors can be given as follows

$$\omega_1 = -U_\psi + U_t \quad (41)$$
$$\omega_2 = U_\psi + U_t \quad (42)$$
$$\omega_3 = |U_\theta| + U_t \quad (43)$$
$$\theta_1 = U_h - sat(U_\phi, U_{\phi max}) \quad (44)$$
$$\theta_2 = U_h + sat(U_\phi, U_{\phi max}) \quad (45)$$
$$\theta_3 = U_\theta \quad (46)$$

where $sat(x_1, x_2)$ is a saturation function that limits x_1 within the range $[-x_2, x_2]$ and $U_{\phi max}$ is the maximum allowed U_ϕ to avoid stall of main wings. The tilt angles of right and left servo motors θ_1, θ_2 determine the moment creating roll operation in horizontal mode as implied in equation (35). Considering the mechanism of roll operation, output of the PID controller in charge of roll operation U_ϕ goes to the right servo motor with negative sign and goes to the left servo motor. The U_h is the typical angle of attack of fixed wings, which is close to 5°. As a consequence, differential tilt angles of right servo motor with respect to left servo motor creates roll operation described in equation (35). The adjustment of angles θ_1, θ_2 with the bias U_h is not shown in Fig.12(d). In case of pitch operation in equation (36), the output of the PID controller for pitch operation U_θ should be used to determine θ_3, ω_3. Direction of pitch operation, either nose up or nose down, is determined by the thrust vectoring based on θ_3, ω_3, as shown in equation (36). For yaw operation, rotational speed of right BLDC motor ω_1 is $-U_\psi + U_t$ and rotational speed of left BLDC motor ω_2 is $U_\psi + U_t$ as expected. The gains of PID/PI controllers for horizontal flight mode are listed in TABLE 5. The mark "x" in TABLE 5 represents that no gain is assigned.

TABLE 5. Gains of PID/PI controllers for horizontal flight mode.

	K_p	K_i	K_d	K_a	K_{acc}
Roll	0.83	0.15	0.33	15	x
Pitch	7.78	1.36	4.68	x	x
Yaw	61.1	8.1	x	x	0.1

C. TRANSITION PROCESS FOR TESTING

In general, the transition from vertical mode to horizontal mode is problematic with the hybrid UAVs. During this transition, nonlinear aspect of the lift force on the wings introduces undesirable instability of the UAVs. The transition process for testing is conducted in a fashion as follows

1. With a command for the forward transition in the vertical flight mode, proposed UAV starts tilting main wings while the angle of tail BLDC motor is adjusted as much as the tilting angle of the main wings.

2. To avoid instability during tilting main wings, PID controller for pitch operation in horizontal flight mode adjusts the angle of tail BLDC motor simultaneously.

3. Reaction torque of tail motor during forward transition is compensated by wing tilt mechanism controlled by PID controller for vertical flight mode. When the UAV reaches desired airspeed V_{des}, target yaw angle is set to current vehicle heading.

4. When desired airspeed is sustained more than T_{des} seconds, main wings are tilted all the way forward. While main wings are tilted, the angle of tail rotor is adjusted by PID controller for pitch operation.

5. The PID controller for vertical flight mode is switched to the PID controller for horizontal flight mode when main wings laid completely.

By trial-and-errors, it is found that proper values of V_{des} and T_{des} are approximately 10m/s, 2.5s, respectively. Backward transition is conducted by tilting main wings and tail BLDC motor vertically along with switching of the PID/PI controller for horizontal flight mode to the PID controller for vertical flight mode.

Following the forward and backward transitions specified above, mode transition of the proposed UAV is tested in experiments.

V. RESULTS OF SIMULATIONS AND EXPERIMENTS

In this section, the PID controller/PI controller presented in Section IV is implemented by Matlab® and Simulink® for

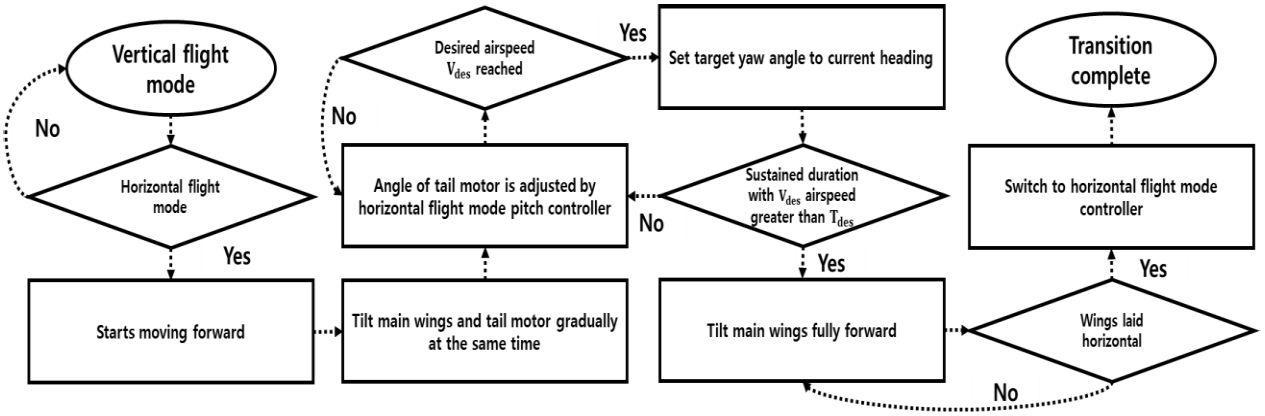

FIGURE 13. Flow chart of forward transition.

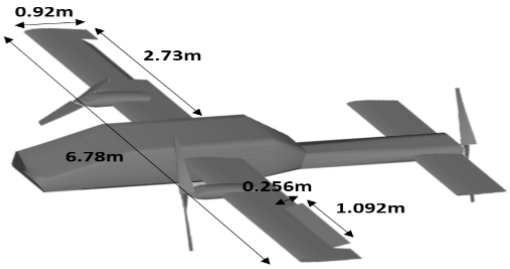

FIGURE 14. UAV with ailerons and propellers used for simulations. Proposed UAV with individual wing control takes the same dimensions as those of this UAV.

simulations and experiments. The X-plane® is used as the flight simulator. Simulation results are mainly to show that the roll rate of the UAV during the cruise flight is significantly increased over the UAV with ailerons. Experimental results are to demonstrate that the UAV can perform various maneuvers successfully.

A. SIMULATIONS OF HORIZONTAL FLIGHT

Effect of individual control of main wings in relation to the control of ailerons is observed by simulations rather than by experiments. For experiments, a replica of the proposed UAV with ailerons, dedicated control circuits for the ailerons, additional actuators, and additional control programs are needed. Simulation results with the UAV capable of separate control of main wings and other UAV with ailerons are obtained for the horizontal mode by X-plane® flight simulator and Matlab/Simulink®. Since flight simulation with small UAV often leads to erroneous behavior of it, the UAV is scaled up as shown in Fig.14. Proportion of the area of the aileron is adjusted to that of Canadair® CL-84. The UAV with individual control of main wings without ailerons and the UAV with ailerons use identical fuselage and main wings. Total weight (mass) of the UAV is 500kg.

Figure 15 shows simulation results obtained in horizontal flight mode. Range of the speed of both UAVs is 75-82m/s, as shown in Fig.15(a). Allowed range of deflection angle of the ailerons is $0° \sim 20°$, which is typical range of practical ailerons. Roll operation with roll angle 70° is commanded by pulse inputs issued with 5s interval when each UAV flies at 80m/s, as seen in Fig.15(b). Duration of each pulse input is 0.5s. Variation of roll and pitch angles of the proposed UAV to meet the target roll angle is shown in Fig.15(b) together with that of the UAV with ailerons. It is shown in Fig.15(b) that the UAV with ailerons cannot execute the command properly. The UAV with ailerons just achieves $50° \sim 60°$ of roll angle, whereas the proposed UAV fulfills the command. In order to execute the command, deflection angles of the main wings of the proposed UAV are $\pm 13°$, while they are $\pm 20°$ with the UAV taking ailerons, as seen Fig.15(c). Small deflection angle of main wings still allows larger difference of lift force of main wings, as seen in Fig.15(d). As seen in Fig.15(c), wing lift force of each main wing, as well as the difference between them, is larger with proposed UAV. Considering that the difference between wing lift forces determines maneuver performance, the proposed UAV can achieve higher efficiency in maneuvering. The maximum roll rate (angular speed) of the proposed UAV in Fig.15(e) is about 2.7rad/s and the UAV with ailerons is about 1.5rad/s, representing 80% improvement obtained by the proposed UAV. The sideslip occurred during the execution of roll operation is shown in Fig.15(f). Thrust forces of the BLDC motors to reduce sideslip are presented in Fig.15(g). For the gain tuning of flight experiments, software in the loop simulation (SILS) stated in [48], [49] is considered for the horizontal flight mode and hardware in the loop simulation (HILS) in [50] is adopted for the vertical flight mode.

B. OUTDOOR FLIGHT EXPERIMENTS

Outdoor flight experiments are conducted with wind disturbance to verify flight stability of the proposed UAV. Target angles are given by an RC transmitter and average wind speed measured by anemometer is 4m/s. Figure 17(a) shows the UAV and Fig.17(b) represents vertical take-off. During the hovering flight shown in Fig.17(c), loiter mode provided by Ardupilot code is used. Loiter mode of the Ardupilot code

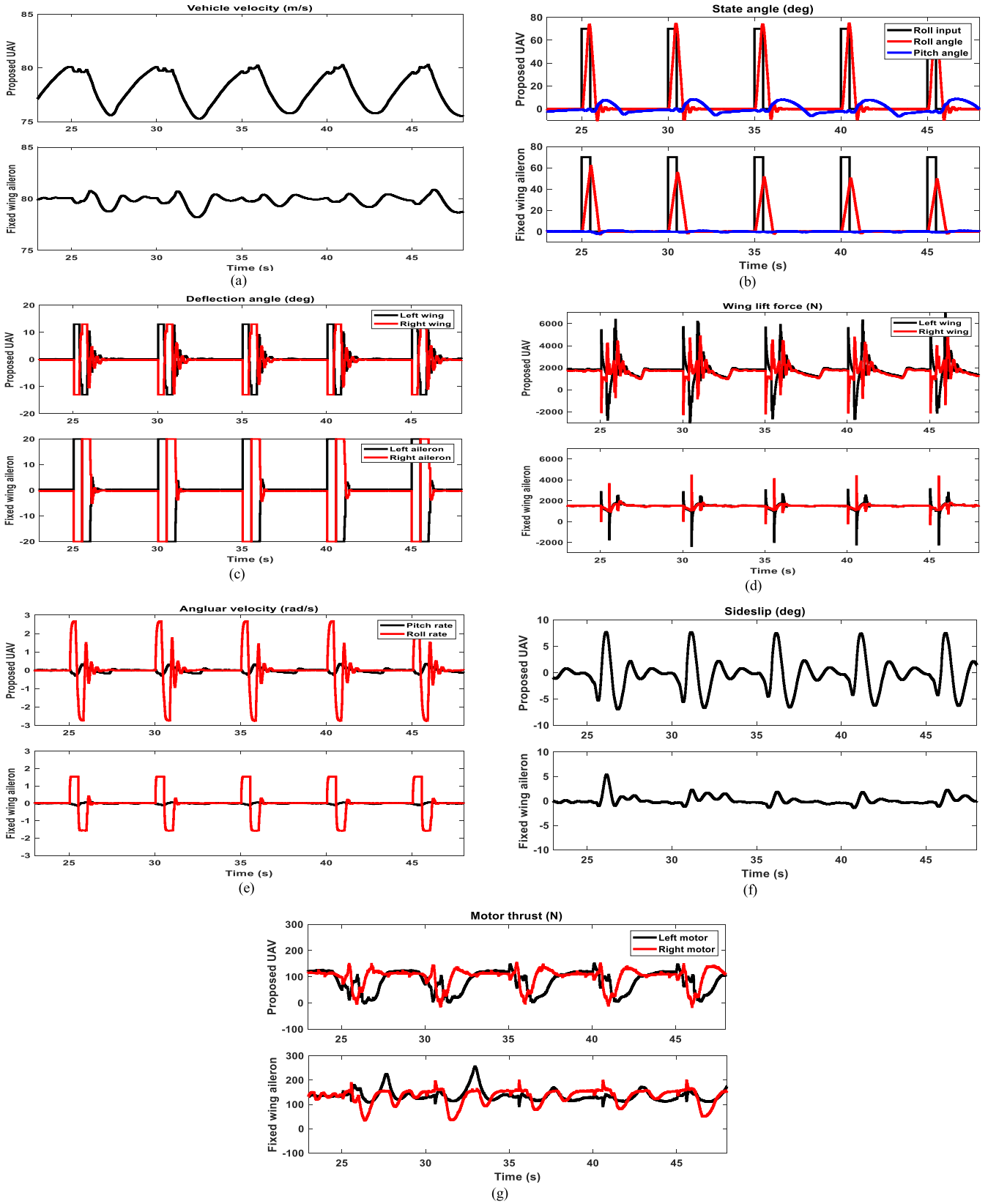

FIGURE 15. Simulation results of horizontal flight with proposed UAV (presented as "Proposed UAV") and UAV with ailerons (Fixed wing aileron): (a) vehicle velocities; (b) pitch and roll angles; (c) deflection angles of wings and ailerons; (d) lift forces of wings; (e) pitch and roll rates; (f) sideslip angle; (g) thrust of the BLDC motors to reduce sideslip.

FIGURE 16. Outdoor flight experiment with wind disturbance: (a) prototype of the UAV; (b) vertical take-off; (c) hovering; (d) vertical flight; (e) forward transition; (f) horizontal flight after forward transition; (g) backward transition.

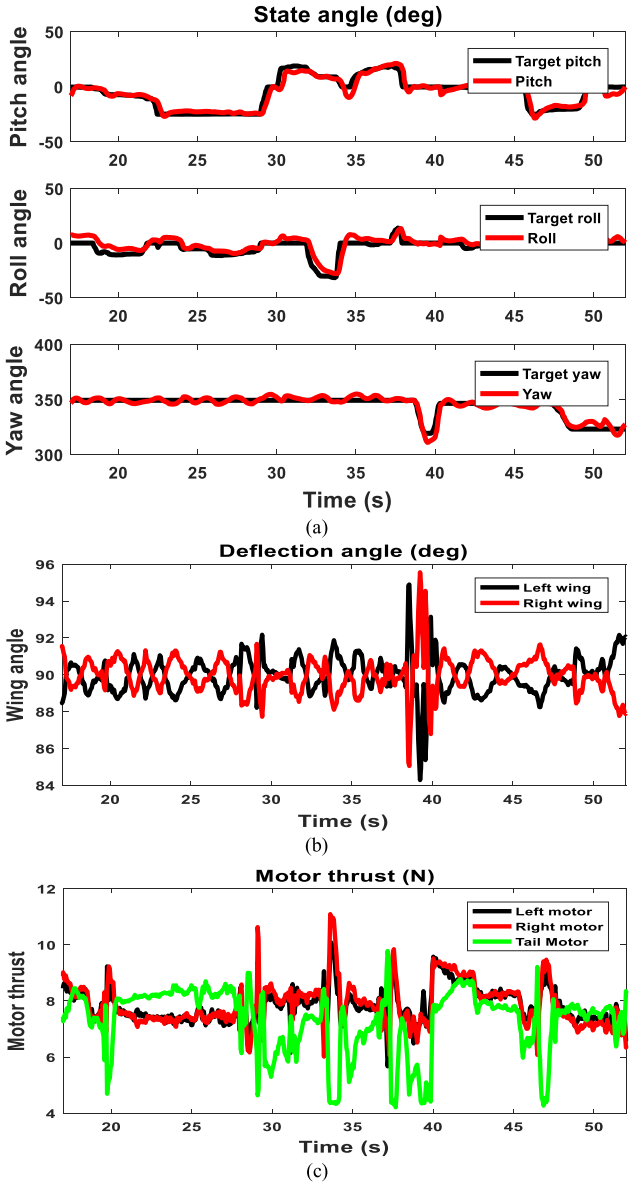

FIGURE 17. Experimental results of vertical flight with proposed UAV: (a) variation of actual pitch, roll, and yaw angles according to their respective target angles; (b) variation of deflection angles of main wings during yaw operation; (c) variation of thrust of each BLDC motor during pitch and roll operations.

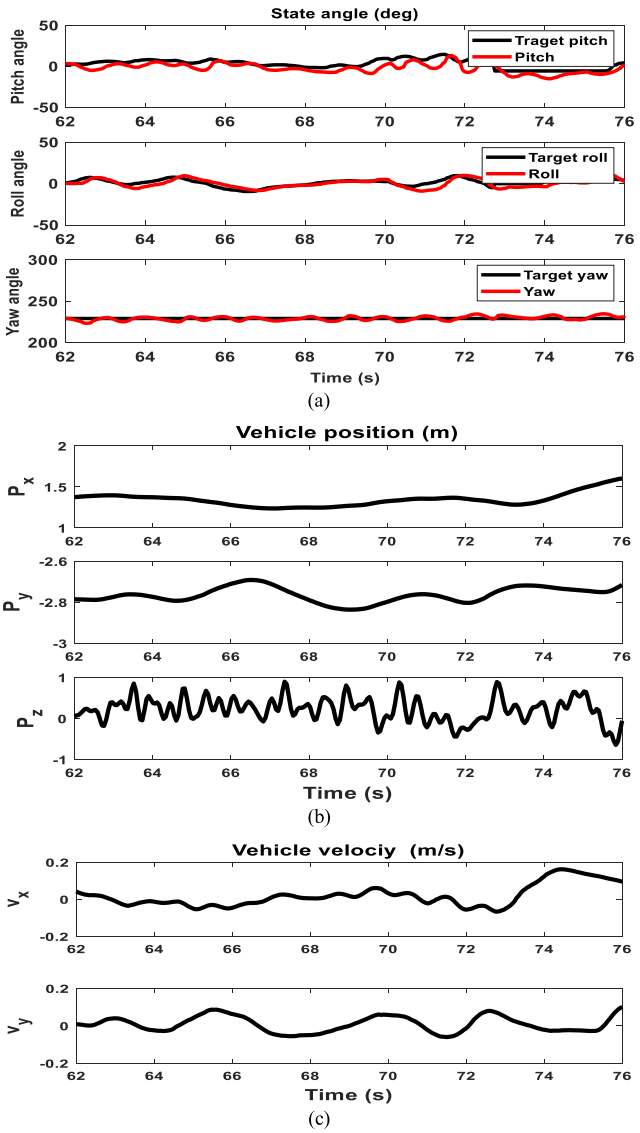

FIGURE 18. Experimental results of hovering flight with wind disturbance: (a) pitch, roll, yaw angles during hovering flight; (b) vehicle position during hovering flight; (c) vehicle speed during hovering flight.

attempts to hold the position of the UAV against wind disturbance. Figure 17(d-g) represent vertical flight, forward transition, horizontal flight after forward transition, and backward transition, respectively. Flight performance in each flight mode is measured by the root mean squared error (RMSE) of pitch, roll, and yaw operations.

C. EXPERIMENTS OF VERTICAL FLIGHT

Experimental results of vertical flight with the proposed UAV are shown in Fig.17. Target angle is set by the RC transmitter. Flight performance in tracking the target angle is seen to be good. A little fluctuation of yaw angle in Fig.17(a) represents the continual compensation of time-varying reaction torque by individually tilted main wings. The deflection angles of the main wings during the yaw operation are shown in Fig.17(b). Variation of thrust of each BLDC motor when performing pitch and roll operations is depicted in Fig.17(c).

D. EXPERIMENTS OF HOVERING FLIGHT WITH WIND DISTURBANCE

Figure 18 shows the hovering flight performance of the UAV. Results of hovering flight show that the proposed UAV is a little vulnerable to the wind disturbance because of large wing surfaces and lightweight of the UAV. However, the proposed UAV tends to hold the vehicle's attitude shown in Fig.18(a) and position shown in Fig.18(b). Though there are fluctuations of pitch, roll, yaw angles and variations of vehicle

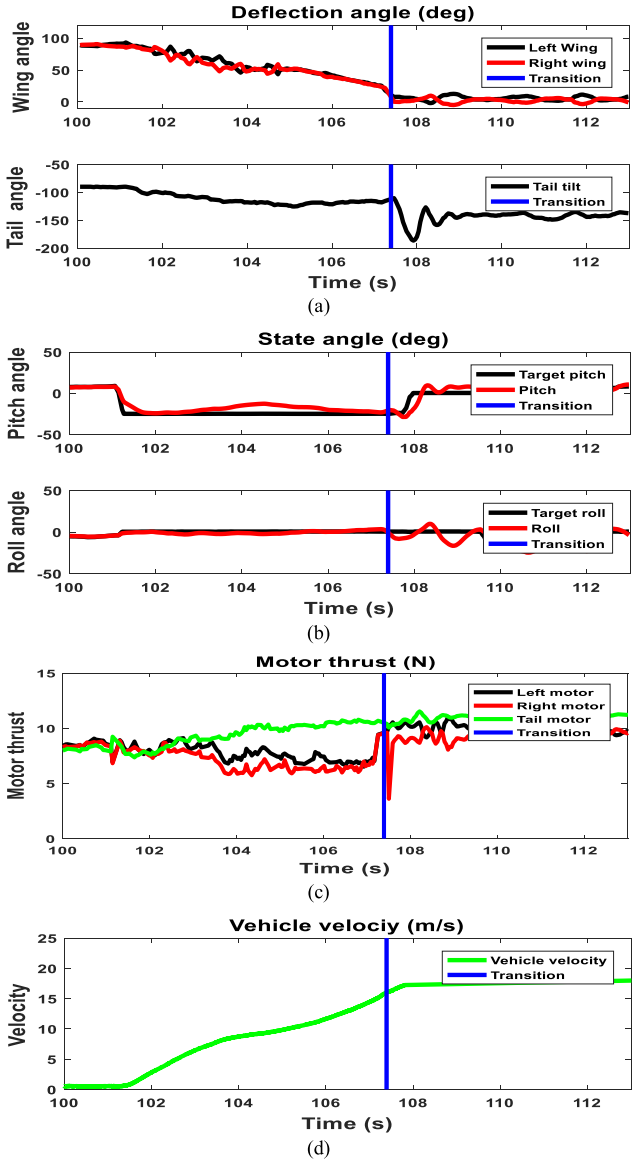

FIGURE 19. Experimental results of forward transition: (a) variation of deflection angle of the main wings and tail motor; (b) variation of pitch and roll angles according to their respective target angles; (c) variation of thrust of each BLDC motor; (d) variation of vehicle speed before and after forward transition.

position, they are bounded within small range. The vehicle position is obtained by the GPS module and barometer in the UAV. The oscillations are caused by wind disturbance, which results in time-varying behavior of UAV attitude and position. From the experimental results, the UAV is expected to perform robustly against wind disturbance with wind speed upto about 5m/s.

E. EXPERIMENTS OF FORWARD TRANSITION

Figure 19 shows experimental result of forward transition. The blue vertical line in each figure represents completion of forward transition. Mode transition is best observed with the variation of deflection angle as shown in Fig. 19(a). The command of the RC transmitter for forward transition is conveyed approximately at the 101th second and then the UAV moves forward with target pitch angle, as shown in Fig. 19(b). Tilting main wings and tail BLDC motor starts gradually and simultaneously. The thrust of each BLDC motor shown in Fig.19(c) is controlled by PID controller for vertical flight mode. To avoid instability during the forward transition, the angle of tail BLDC motor is adjusted by PID controller for pitch operation in horizontal flight mode. When the vehicle reaches target (desired) airspeed V_{des}(10m/s), UAV sets its target yaw angle to its current heading direction. As a result, main wings of the proposed UAV stop oscillation and gradually lays horizontal. When the desired airspeed is sustained more than 2.5 seconds, main wings are tilted fully forward and the PID controller for vertical flight mode is switched to PID/PI controller for horizontal flight mode. The forward transition is complete roughly at the 108th second. Because the pitch angle of the UAV corresponds with the target pitch angle, as shown in Fig.19(b), the proposed UAV seems to have sustained stability during the forward transition.

F. EXPERIMENTS OF HORIZONTAL FLIGHT

The result of the horizontal flight is shown in Fig.20. The attitude of vehicle is controlled by tilting main wings and tail motor, as shown in Fig.20(a). By this tilting mechanism, proposed UAV keeps stabilizing its attitude as seen in Fig.20(b). According to the deflection angles of main wings, proposed UAV operates roll maneuver in the horizontal flight. Variation of the thrust of each BLDC motor is shown in Fig.20(c). The speed of the UAV shown in Fig.20(d) can reach 20m/s in the horizontal flight mode.

G. EXPERIMENTS OF BACKWARD TRANSITION

Figure 21 shows experimental results obtained from backward transition procedure. The blue vertical line in each figure represents completion of backward transition. The backward transition starts approximately at 128th second with erecting main wings and tail motor vertically, as shown in Fig.21(a). Variation of pitch and roll angles according to their respective target angles is shown in Fig.21(b). By the command of backward transition, the thrust of each BLDC motor quickly drops to 0, as shown in Fig.21(c). After the completion of backward transition, the UAV is controlled by the PID controller for vertical flight mode. By the backward transition, the speed of the UAV is rapidly decreased, as shown in Fig.21(d).

Flight performance can be measured by the root mean squared error (RMSE) of pitch, roll, and yaw operations during the flight operations in Fig.17(a), Fig.18(a), Fig.19(b), Fig.20(b), Fig.21(b). The RMSE values are listed in TABLE 6. The sample interval in the figures is 0.05s. The error represents the difference between target angle and achieved angle. The "Duration" in the first row of TABLE 6 indicates the time interval where the statistic RMSE is evaluated. It is seen in TABLE 6 that the average RMSE is

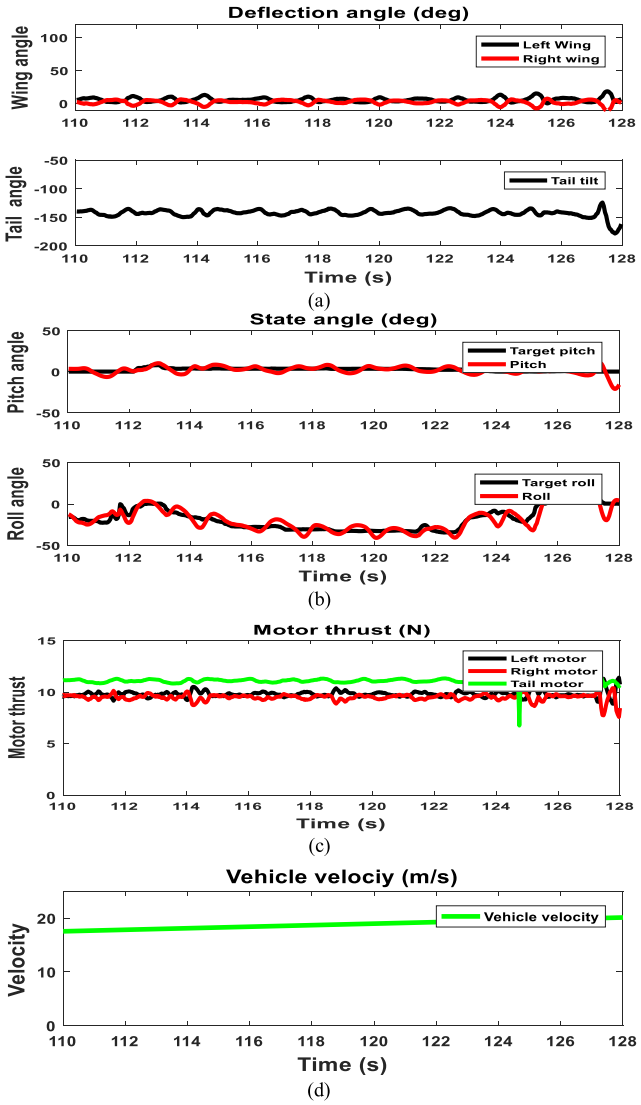

FIGURE 20. Experimental results of horizontal flight: (a) variation of deflection angle of main wings and tail motor; (b) variation of pitch and roll angles according to their respective target angle; (c) variation of thrust of each BLDC motor; (d) variation of vehicle speed during the horizontal flight.

TABLE 6. RMSE of pitch, roll, yaw operations.

	Vertical Flight Fig.17(a)	Hovering Fig.18(a)	Forward Transition Fig.19(b)	Horizontal Flight Fig.20(b)	Backward Transition Fig.21(b)
Duration (s)	17~52	62~76	101~108	108~128	128~129
Pitch (deg)	3.8133	6.1837	6.6734	4.0572	7.4447
Roll (deg)	4.4500	4.1465	2.4397	6.3032	8.4655
Yaw (deg)	2.9900	2.8129			

the smallest with yaw operation whereas it is the largest with pitch operation. Except for the backward transition, overall maneuver performance is seen to be moderately good or better. Relatively large value of the RMSE with the backward transition is due to the small fluctuation over time interval 128-129s in Fig.21(b).

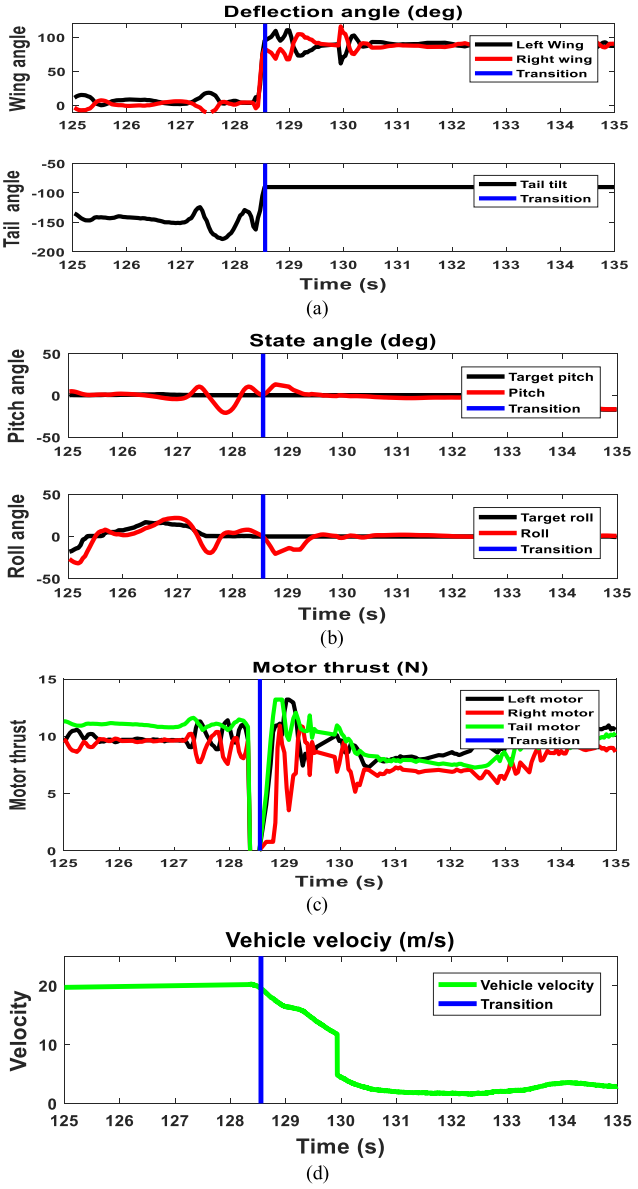

FIGURE 21. Experimental results of backward transition: (a) variation of deflection angle of the main wings and tail motor; (b) variation of pitch and roll angles according to their respective target angles; (c) variation of thrust of each BLDC motor; (d) variation of vehicle speed before and after backward transition.

VI. CONCLUSION

This paper presents a tri-copter type of tilt wing UAV featured by individual control of main wings. The proposed UAV can make attitude operations by thrust vectoring of two motors on main wings and a tail motor or by thrust vectoring combined with control of the directions of main wing surfaces. Thrust vectoring of motors and changing the direction of wing surfaces can be achieved by tilting main wings individually. The UAV is also able to compensate reaction torque, which is a typical problem of tri-copter type UAVs, by tilting each main wing individually. Tilting main wings individually can generate large difference of aerodynamic lift force on the main wings, thereby allowing various maneuvers of the UAV.

Dynamic model of the proposed UAV is established via the Newton-Euler formulation and effect of individual wing control is examined by simulations and experiments. The PID controller and PI controller for attitude control are implemented and used for simulations and experiments. Results of simulations and experiments are presented for validation of flight performance of the developed UAV, including the roll rate of the proposed UAV 80% larger than the conventional UAV with ailerons as control surfaces.

REFERENCES

[1] H. Bendea, P. Boccardo, S. Dequal, F. G. Tonolo, D. Marenchino, and M. Piras, "Low cost UAV for post-disaster assessment," in *Proc. Congr. Int. Soc. Photogramm. Remote Sens.*, Jan. 2008, pp. 1373–1380.

[2] M. Petrolo, E. Carrera, M. D'Ottavio, C. de Visser, Z. Patek, and Z. Janda, "On the development of the anuloid, a disk-shaped VTOL aircraft for urban areas," *Adv. Aircr. Spacecraft Sci.*, vol. 1, no. 3, pp. 353–378, Jul. 2014.

[3] J. Abras and R. Narducci, "Analysis of CFD modeling techniques over the MV-22 tiltrotor," in *Proc. 66th Annu. Forum Am. Helicopter Soc.*, Jan. 2010, pp. 11–13.

[4] J. E. Naranjo, M. Clavijo, F. Jimenez, O. Gomez, J. L. Rivera, and M. Anguita, "Autonomous vehicle for surveillance missions in off-road environment," in *Proc. IEEE Intell. Vehicles Symp.*, Jun. 2016, pp. 98–103.

[5] M. Hochstenbach, C. Notteboom, B. Theys, and J. De Schutter, "Design and control of an unmanned aerial vehicle for autonomous parcel delivery with transition from vertical take-off to forward flight—VertiKUL, a quadcopter tailsitter," *Int. J. Micro Air Veh.*, vol. 7, no. 4, pp. 395–405, Dec. 2015.

[6] P. Bourdin, A. Gatto, and M. I. Friswell, "Performing co-ordinated turns with articulated wing-tips as multi-axis control effectors," *Aeronaut. J.*, vol. 114, no. 1151, pp. 35–47, Jan. 2010.

[7] Z. Ren, W. Fu, Y. Li, B. Yan, S. Zhu, and J. Yan, "Enhanced attitude control of unmanned aerial vehicles based on virtual angular accelerometer," *IEEE Access*, vol. 7, pp. 104330–104343, 2019.

[8] M. Rabah, A. Rohan, S. A. S. Mohamed, and S.-H. Kim, "Autonomous moving target-tracking for a UAV quadcopter based on fuzzy-PI," *IEEE Access*, vol. 7, pp. 38407–38419, 2019.

[9] A. S. Saeed, A. B. Younes, S. Islam, J. Dias, L. Seneviratne, and G. Cai, "A review on the platform design, dynamic modeling and control of hybrid UAVs," in *Proc. Int. Conf. Unmanned Aircr. Syst. (ICUAS)*, Jun. 2015, pp. 806–815.

[10] M. Hassanalian and A. Abdelkefi, "Classifications, applications, and design challenges of drones: A review," *Progr. Aerosp. Sci.*, vol. 91, pp. 99–131, May 2017.

[11] G. Cai, B. M. Chen, T. H. Lee, and M. Dong, "Design and implementation of a hardware-in-the-loop simulation system for small-scale UAV helicopters," *Mechatronics*, vol. 19, no. 7, pp. 1057–1066, Oct. 2009.

[12] E. Cetinsoy, C. Hancer, K. T. Oner, E. Sirimoglu, and M. Unel, "Aerodynamic design and characterization of a quad tilt-wing UAV via wind tunnel tests," *J. Aerosp. Eng.*, vol. 25, no. 4, pp. 574–587, Oct. 2012.

[13] P. Gnemmi, S. Changey, K. Meder, E. Roussel, C. Rey, C. Steinbach, and C. Berner, "Conception and manufacturing of a projectile-drone hybrid system," *IEEE/ASME Trans. Mechatronics*, vol. 22, no. 2, pp. 940–951, Apr. 2017.

[14] U. Ozdemir, Y. O. Aktas, A. Vuruskan, Y. Dereli, A. F. Tarhan, K. Demirbag, A. Erdem, G. D. Kalaycioglu, I. Ozkol, and G. Inalhan, "Design of a commercial hybrid VTOL UAV system," *J. Intell. Robotic Syst.*, vol. 74, nos. 1–2, pp. 371–393, Oct. 2013.

[15] D. Cabecinhas, R. Naldi, L. Marconi, C. Silvestre, and R. Cunha, "Robust take-off for a quadrotor vehicle," *IEEE Trans. Robot.*, vol. 28, no. 3, pp. 734–742, Jun. 2012.

[16] A. M. Stoll, E. V. Stilson, J. Bevirt, and P. P. Pei, "Conceptual design of the joby s2 electric VTOL PAV," in *Proc. 14th AIAA Aviation Technol. Integr. Oper. Conf.*, Jun. 2014, pp. 16–20.

[17] S. Srigrarom, W. K. Teo, J. K. Quek, and J. J. Lim, "Development of flight control for UGS Tri-copter MAV," *J. Unmanned Syst. Technol. Dev.*, vol. 4, no. 1, pp. 1–8, 2016.

[18] S. Suzuki, "Attitude control of quad rotors QTW-UAV with tilt wing mechanism," *J. Syst. Des. Dyn.*, vol. 4, no. 3, pp. 416–428, 2010.

[19] J. Holsten, T. Ostermann, Y. Dobrev, and D. Moormann, "Model validation of a tiltwing Uav in transition phase applying windtunnel investigations," in *Proc. 28th Int. Congr. Aeronaut. Sci.*, 2012, pp. 1–10.

[20] Y. Jung and D. H. Shim, "Development and application of controller for transition flight of tail-sitter UAV," *J. Intell. Robot. Syst. Theory Appl.*, vol. 65, no. 1, pp. 137–152, Jan. 2012.

[21] A. Oosedo, A. Konno, T. Matumoto, K. Go, K. Masuko, S. Abiko, and M. Uchiyama, "Design and simulation of a quad rotor tail-sitter unmanned aerial vehicle," in *Proc. IEEE/SICE Int. Symp. Syst. Integr.*, Dec. 2010, pp. 254–259.

[22] O. Garcia, P. Castillo, K. C. Wong, and R. Lozano, "Attitude stabilization with real-time experiments of a tail-sitter aircraft in horizontal flight," *J. Intell. Robot. Syst. Theory Appl.*, vol. 65, no. 1, pp. 123–136, Aug. 2012.

[23] Y. Ke, K. Wang, and B. M. Chen, "Design and implementation of a hybrid UAV with model-based flight capabilites," *IEEE/ASME Trans. Mechatronics*, vol. 23, no. 3, pp. 1114–1125, Jan. 2018.

[24] K. Z. Y. Ang, J. Cui, T. Pang, K. Li, K. Wang, Y. Ke, and B. M. Chen, "Development of an unmanned tail-sitter with reconfigurable wings: U-lion," in *Proc. 11th IEEE Int. Conf. Control Autom. (ICCA)*, Jun. 2014, pp. 750–755.

[25] J. Escareño, A. Sanchez, O. Garcia, and R. Lozano, "Modeling and global control of the longitudinal dynamics of a coaxial convertible mini-UAV in hover mode," *J. Intell. Robot. Syst. Theory Appl.*, vol. 54, no. 2, pp. 261–273, Mar. 2009.

[26] A. Vargas-Clara and S. Redkar, "Dynamics and control of a stop rotor unmanned aerial vehicle," *Int. J. Electr. Comput. Eng.*, vol. 2, no. 5, pp. 2088–8708, Oct. 2012.

[27] C. W. Acree, Jr., H. Yeo, and J. Sinsay, "Performance optimization of the NASA large civil tiltrotor," in *Proc. Nati. Aeron. Spac. Admin. Moff. Fiel. Caam. Resear. Cent.*, Jul. 2008, pp. 1–14.

[28] T. Ostermann, J. Holsten, Y. Dobrev, and D. Moormann, "Control concept of a tiltwing UAV during low speed manoeuvring," in *Proc. 28th Int. Congr. Aeronaut. Sci.*, 2012, pp. 1–10.

[29] K. Muraoka, N. Okada, D. Kubo, and M. Sato, "Transition flight of quad tilt wing Vtol Uav," in *Proc. 28th Int. Congr. Aeronaut. Sci.*, 2012, pp. 1–10.

[30] G. Heredia, A. Duran, and A. Ollero, "Modeling and simulation of the HADA reconfigurable UAV," *J. Intell. Robot. Syst. Theory Appl.*, vol. 65, no. 1, pp. 115–122, Jan. 2012.

[31] I. Palunko, P. Cruz, and R. Fierro, "Agile load transportation?: Safe and efficient load manipulation with aerial robots," *IEEE Robot. Autom. Mag.*, vol. 19, no. 3, pp. 69–79, Sep. 2012.

[32] D.-W. Yoo, H.-D. Oh, D.-Y. Won, and M.-J. Tahk, "Dynamic modeling and stabilization techniques for tri-rotor unmanned aerial vehicles," *Int. J. Aeronaut. Space Sci.*, vol. 11, no. 3, pp. 167–174, Sep. 2010.

[33] C. Papachristos and A. Tzes, "Modeling and control simulation of an unmanned tilt tri-rotor aerial vehicle," in *Proc. IEEE Int. Conf. Ind. Technol.*, Mar. 2012, pp. 840–845.

[34] D. Anh Ta, I. Fantoni, and R. Lozano, "Modeling and control of a tilt tri-rotor airplane," in *Proc. Amer. Control Conf. (ACC)*, Jun. 2012, pp. 131–136.

[35] F. Kendoul and I. Fantoni, "Modeling and control of a small autonomous aircraft having two tilting rotors," *IEEE Trans. Robot.*, vol. 22, no. 6, pp. 1297–1302, Dec. 2006.

[36] E. Cetinsoy, S. Dikyar, C. Hancer, K. T. Oner, E. Sirimoglu, M. Unel, and M. F. Aksit, "Design and construction of a novel quad tilt-wing UAV," *Mechatronics*, vol. 22, no. 6, pp. 723–745, Sep. 2012.

[37] T. Mikami and K. Uchiyama, "Design of flight control system for quad tilt-wing UAV," in *Proc. Int. Conf. Unmanned Aircr. Syst. (ICUAS)*, Jun. 2015, pp. 801–805.

[38] V. Hrishikeshavan, C. Bogdanowicz, and I. Chopra, "Design, performance and testing of a quad rotor biplane micro air vehicle for multi role missions," *Int. J. Micro Air Vehicles*, vol. 6, no. 3, pp. 155–173, Sep. 2014.

[39] D. Raymer, *Aircraft Design: A Conceptual Approach*, 6th ed. Reston, VA, USA: American Institute of Aeronautics and Astronautics, 2019.

[40] V. S. Chipade, Abhishek, M. Kothari, and R. R. Chaudhari, "Systematic design methodology for development and flight testing of a variable pitch quadrotor biplane VTOL UAV for payload delivery," *Mechatronics*, vol. 55, pp. 94–114, Nov. 2018.

[41] Airfoiltools. (2019). *NACA M18 AIRFOIL (M18-IL)*. Accessed: Jan. 8, 2019. [Online]. Available: http://airfoiltools.com/airfoil/details?airfoil=m18-il

[42] R. Kumar, A. Nemati, M. Kumar, R. Sharma, K. Cohen, and F. Cazaurang, "Tilting-rotor quadcopter for aggressive flight maneuvers using differential flatness based flight controller," in *Proc. ASME Dyn. Syst. Control Conf.*, vol. 3, pp. 1–10, Oct. 2017.
[43] A. Alkamachi and E. Erçelebi, "A proportional derivative sliding mode control for an overactuated quadcopter," *Proc. Inst. Mech. Eng., G, J. Aerosp. Eng.*, vol. 233, no. 4, pp. 1354–1363, Jan. 2018.
[44] M. Ryll, H. H. Bulthoff, and P. R. Giordano, "A novel overactuated quadrotor unmanned aerial vehicle: Modeling, control, and experimental validation," *IEEE Trans. Control Syst. Technol.*, vol. 23, no. 2, pp. 540–556, Mar. 2015.
[45] A. Nemati, R. Kumar, and M. Kumar, "Stabilizing and control of tilting-rotor quadcopter in case of a propeller failure," in *Proc. ASME Dyn. Syst. Control Conf.*, vol. 1, pp. 1–8, Oct. 2016.
[46] R. Kumar, S. Sridhar, F. Cazaurang, K. Cohen, and M. Kumar, "Reconfigurable fault-tolerant tilt-rotor quadcopter system," in *Proc. ASME Dyn. Syst. Control Conf.*, vol. 3, pp. 1–10, Oct. 2018.
[47] J. W. Langelaan, N. Alley, and J. Neidhoefer, "Wind field estimation for small unmanned aerial vehicles," *J. Guid., Control, Dyn.*, vol. 34, no. 4, pp. 1016–1030, Jul. 2011.
[48] A. Bittar, H. V. Figuereido, P. A. Guimaraes, and A. C. Mendes, "Guidance Software-In-the-Loop simulation using X-Plane and simulink for UAVs," in *Proc. Int. Conf. Unmanned Aircr. Syst. (ICUAS)*, May 2014, pp. 993–1002.
[49] A. Bittar and N. M. F. de Oliveira, "Hardware-in-the-loop simulation of an attitude control with switching actuators for SUAV," in *Proc. Int. Conf. Unmanned Aircr. Syst. (ICUAS)*, May 2013, pp. 134–142.
[50] K. D. Nguyen and C. Ha, "Development of hardware-in-the-loop simulation based on gazebo and pixhawk for unmanned aerial vehicles," *Int. J. Aeronaut. Space Sci.*, vol. 19, no. 1, pp. 238–249, Apr. 2018.

KYUNG-JAE NAM received the B.Sc. degree in mechanical engineering from Inha University, South Korea, in 2018. He is currently pursuing the M.S. degree with the Cho Chun Shik Graduate School of Green Transportation, Korea Advanced Institute of Science and Technology. His research interest includes the development of airway transportation systems.

JOOSANG JOUNG is currently pursuing the B.Sc. degree in aerospace engineering with the Korea Advanced Institute of Science and Technology. His research interest includes the development of airway transportation systems.

DONGSOO HAR (Senior Member, IEEE) received the B.Sc. and M.Sc. degrees in electronics engineering from Seoul National University, respectively, and the Ph.D. degree in electrical engineering from Polytechnic University, Brooklyn, NY, USA. He is currently a Faculty Member with the Korea Advanced Institute of Science and Technology (KAIST). He authored and published more than 100 articles in international journals and conferences. His main research interest includes the development of intelligent transportation systems. He was a member of advisory board, the Program Chair, the Vice Chair, and the General Chair for international conferences. He was a recipient of the Best Paper Award (Jack Neubauer Award) from the IEEE TRANSACTIONS ON VEHICULAR TECHNOLOGY, in 2000. He is an Associate Editor of the IEEE SENSORS JOURNAL. He also presented invited talks and keynote in international conferences.